Basin Research

IAS EAGE

Basin Research (2013) **25**, 613–637, doi: 10.1111/bre.12019

Pleistocene landscape entrenchment: a geomorphological mountain to foreland field case, the Las Tunas system, Argentina

E. Pepin,* S. Carretier,* G. Hérail,* V. Regard,† R. Charrier,† M. Farías,‡ V. García§ and L. Giambiagi¶

**Geosciences Environnement Toulouse, OMP, UPS, CNRS, IRD, Université de Toulouse, Toulouse, France*
†U. de Chile, Advanced Mining Technology Center (AMTC), Facultad de Ciencias Físicas y Matemáticas; U. Andres Bello, Escuela de Ciencias de la Tierra, Facultad de Ingeniería, Santiago de Chile, Chile
‡U. de Chile, Departamento de Geología, Facultad de Ciencias Físicas y Matemáticas, Santiago de Chile, Chile
§U. Nacional de Río Negro, Inst. de Investigación en Paleobiología y Geología Sede Alto Valle, General Roca, Argentina
¶CCT-Unidad de Tectónica, Instituto Argentino de Nivología, Glaciología y Ciencias Ambientales, Mendoza, Argentina

ABSTRACT

The study of the Las Tunas River incisions, located in the eastern Andean foreland front (33°20' S in Argentina), provides new clues for the interpretation of deep piedmont entrenchments. Both the Las Tunas mountain catchment and its piedmont are strongly entrenched with maximal incision of over 100 m at the mountain front. Three main terrace levels are well exposed and are labelled T1, T2 and T3 from the youngest to the oldest. We combined geological and geomorphological field observations, kinematic GPS data, satellite data and aerial photos with geochronological $^{40}Ar/^{39}Ar$ and ^{10}Be analysis to provide a detailed description of terrace organization and a discussion of the evolution of the Las Tunas landscape. The surprisingly constant ^{10}Be concentrations in surface layers as deep as 1.5 m show that gently dipping alluvial surfaces can be continuously and deeply mixed. Our data show a first period of deposition (Mesones Fm) before 0.85 Myr (minimum T3 age), followed by deep erosion and a second sedimentation period (Las Tunas Fm) that includes a ca. 0.6 Myr ash deposit. T2 and T1 are inset in the Las Tunas Fm and were abandoned ca. 15–20 kyr ago. The similar ages for T2 and T1 show that post-20 *kyr* entrenchment occurred very rapidly. Despite Quaternary deformation in the Las Tunas piedmont, terrace entrenchment is best explained by paleo-climatic changes. The terrace organization reveals that the erosion-sedimentation phases affected the entire system from the piedmont toe to 10 km upstream of the mountain front. Finally, contrary to the neighbouring more deeply incised Diamante River system, where late Quaternary piedmont uplift is more likely to have been a factor causing incision, the more stable Las Tunas system provides an incomplete geomorphological record of Pleistocene and Holocene climate variations. We suggest that climate variations are better recorded in uplifting piedmonts than in stable ones, where the magnitude of incision and sedimentation and the fact that they occur repeatedly at the same elevation can erase a large part of the record.

INTRODUCTION

River entrenchments have been widely studied in recent decades. However, since the early work of Eckis (1928), the causes of river incision have remained unclear and much debated. Many studies have provided links between entrenchment and external forcings such as climatic fluctuations (e.g. Bull, 1964; Beaumont, 1972; Ono, 1990; Poisson and Avouac, 2004; Regard *et al.*, 2006, Dühnforth *et al.*, 2008), tectonic uplift (e.g. Lavé and Avouac, 2001; Viseras *et al.*, 2003) and base level changes (e.g. Blissenbach, 1954; Merritts *et al.*, 1994; Harvey, 1999; Muto and Steel, 2004). As they record integrated river dynamics over many millennia, alluvial aprons and piedmont fans/terraces are important landforms for establishing the link between entrenchment and external forcing. For this reason, they have been extensively studied. Papers dealing with the nature of sediment and stratigraphy (e.g. Blissenbach, 1954; Hooke, 1968;

Correspondence: E. Pepin, Geosciences Environnement Toulouse, OMP, 14 rue E. Belin, Toulouse, France, E-mail: emilie.pepin@geosci1.net

White, 1991; Whipple and Dunne, 1992; Blair, 1999a, b,c) or the dissected vs. undissected relief and landform organization (e.g. Viseras *et al.*, 2003; Staley *et al.*, 2006; Quigley *et al.*, 2007; Volker *et al.*, 2007; Dühnforth *et al.*, 2008; Singh and Tandon, 2010) of alluvial-fan deposits have yielded interesting clues to the origin of sedimentation/erosion phases in a piedmont.

However, two major limitations still prevent the establishment of clear qualitative and quantitative relationships between fan entrenchment and external forcing. Firstly, recent studies show that fan entrenchment can occur without any external changes (e.g. Muto and Steel, 2004; Nicholas and Quine, 2007; Clarke *et al.*, 2010; Pepin *et al.*, 2010, Kim and Jerolmack, 2008; Powell *et al.*, 2012). Secondly, recent numerical and experimental studies have shown strong interconnections between the mountain that supplies sediments and the piedmont that accommodates them (e.g. Humphrey and Heller, 1995; Tucker and Slingerland, 1997; Babault *et al.*, 2005; Carretier and Lucazeau, 2005; Densmore *et al.*, 2007; Pepin *et al.*, 2010; Armitage *et al.*, 2011). These interconnections and autocyclic behaviour confuse the links between external forcing and piedmont entrenchment because they modify the catchment-fan response time to external changes (Babault *et al.*, 2005). For instance, they could induce delays of up to 1 Myr between mountain perturbation and alluvial fan response (Pepin *et al.*, 2010; Armitage *et al.*, 2011).

The main goal of this article is to analyse the origin of terrace formation and entrenchment along a mountain-to-piedmont system. Such an analysis should allow the discussion of the significance of the alluvial records and the reconstruction of the geomorphological history of the landscape. This field study provides new clues to help understand interconnections between mountain and piedmont areas and to estimate the role of external changes.

We chose the Las Tunas field site on the Andean mountain front of Argentina because (1) several terrace levels are exceptionally well defined in the landscape, (2) the terraces occur both in the mountains and the piedmont, (3) the regional tectonic history is relatively well known (e.g. Polanski, 1963; Cristallini *et al.*, 2000, Giambiagi *et al.*, 2003), (4) a major section of the system is a military training ground preserved from farming processes and exploitation for buildings and (5) the neighbouring Diamante River system, 200 km south of Las Tunas, has been studied and can be used for comparison (Baker *et al.*, 2009).

We have carried out detailed topographic surveys combined with field observations and examined satellite data and aerial photographs in order to clarify the terrace geometry and river entrenchment. The resulting data provide evidence for erosion wave propagation and a description of the landscape evolution. We used $^{40}Ar/^{39}Ar$ dating of volcanic ashes interbedded with the sediments and Terrestrial Cosmogenic Nuclide (TCN) ^{10}Be analysis (using both surface samples and depth profiles) to date the morphological surfaces. Finally, we synthesized our data to reconstruct the Pleistocene-Holocene evolution of the Las Tunas system, including the cut and fill cycles, and to propose that climate is the predominant factor controlling the evolution of the Holocene system.

THE LAS TUNAS AREA

Regional structural description

The Las Tunas catchment-fan system is located about 100 km SSW of Mendoza (Fig. 1), between latitudes 33°00′ S and 33°40′ S, in the transition zone between the flat and normal subduction segments of the southern Central Andes (e.g. Stauder, 1975; Cahill and Isacks, 1992; Giambiagi *et al.*, 2001, 2003). This first order geometry is responsible for the morphostructural differences from north to south in the Las Tunas region (Ramos *et al.*, 2002). North of 33° S, a flat-slab subduction led to eastward propagating deformation of the Cordillera lacking a magmatic arc. From west to east, the Andean range in this region consists of the following N-S oriented morphostructural units: the Coastal Cordillera, the Principal Cordillera, the Frontal Cordillera, the Pre-Cordillera and finally the Sierras Pampeanas (Fig. 1). The Progressive uplift of these ranges from west to east occurred since 20 Myr (Giambiagi *et al.*, 2001; Ramos *et al.*, 2002; Giambiagi *et al.*, 2003) and active deformation is present in the piedmont (Ramos *et al.*, 2002; Siame *et al.*, 2005; Siame and Bellier, 2006; Verges *et al.*, 2007). Normal subduction south of 34° S led to the development of the Principal and Frontal Cordillera uplifts with an active magmatic arc. There are no Pre-Cordillera or Sierras Pampeanas structures in this area, indicating that the piedmont is less affected by deformation than in the areas more to the north. The Las Tunas system is thus located in a transitional area between these two segments (Cahill and Isacks, 1992; Giambiagi *et al.*, 2001, 2003).

Between 32° S and 35° S, post-Early Miocene deformation of the Cordillera has been described by Giambiagi *et al.* (2001); Charrier *et al.* (2002); Ramos *et al.* (2002); Giambiagi *et al.* (2003) and Farías *et al.* (2008, 2010). Intense compression between approx. 23 and 16 Myr was responsible for the uplift of the western side of the Principal Cordillera. Since then, deformation migrated eastward and uplift of the Frontal Cordillera occurred in this region at 8–9 Myr. However, it has been shown that uplift of the Frontal Cordillera occurred earlier in the north and propagated gradually southwards. Finally, since ca. 2 Myr the foreland, called the Cuyo basin, has been deformed (Cristallini *et al.*, 2000; Giambiagi *et al.*, 2003), producing structures at the latitude of the Las Tunas region such as the Ventana/Viscacheras blocks, the Barrancas folds and the La Pilona folds (see Fig. 1).

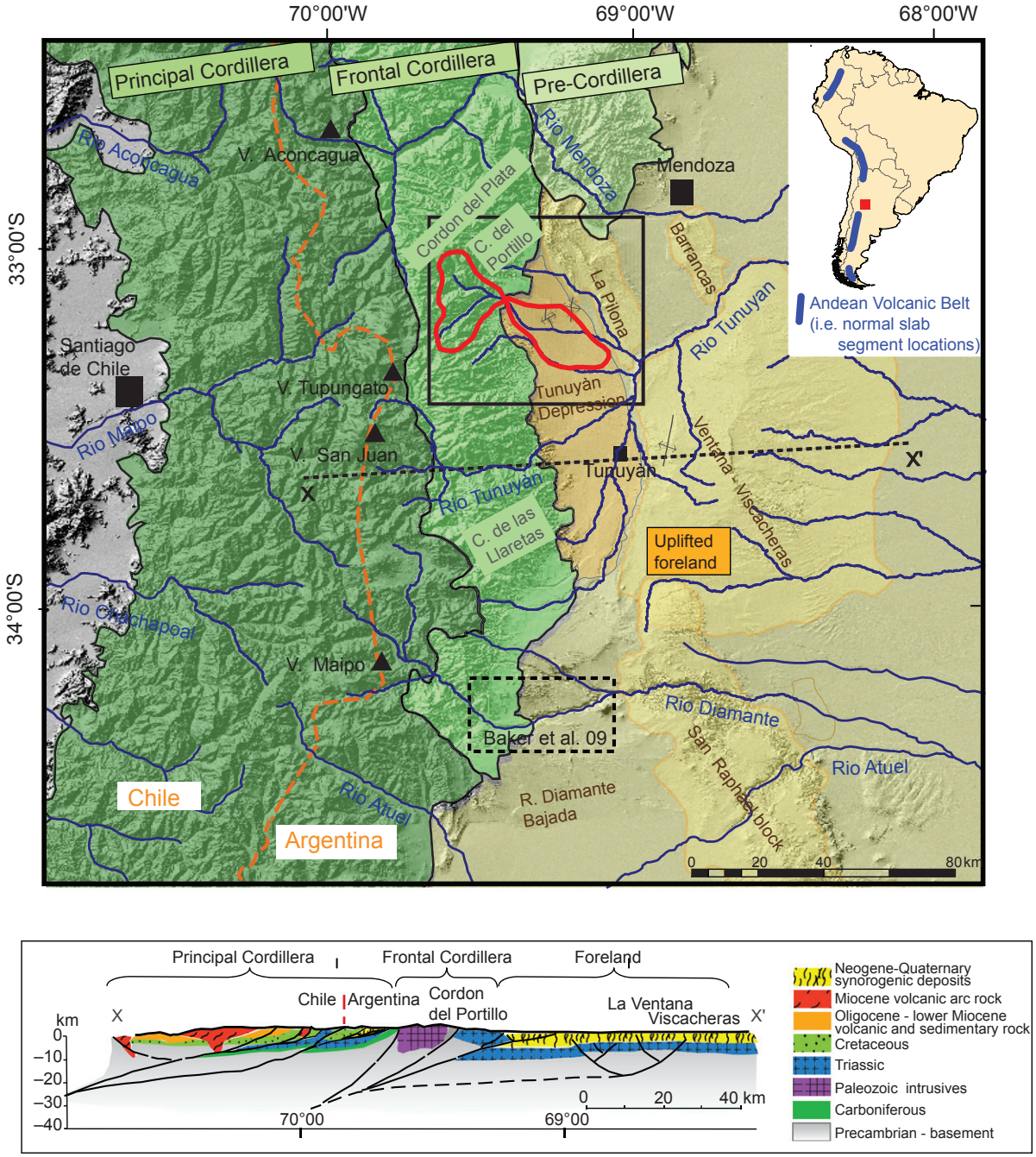

Fig. 1. Regional map of the Las Tunas area and structural interpretation along profile XX' modified from Cristallini *et al.* (2000) and Giambiagi *et al.* (2003). The Las Tunas catchment-fan system is outlined in red, the Cordilleras are green and the foreland is yellow. The black box indicates the location of Fig. 2. The dashed black box indicates the study area of Baker *et al.* (2009) along the Diamante River.

Present-day climate

The rain-shadow effect of the Andes on the westerly winds from the Pacific is responsible for an arid to semi-arid climate (Polanski, 1963; Hoffmann, 1975; D 'Antoni, 1983). Annual maximal temperatures occur in February and are around 33° C in the piedmont area between the Diamante and Mendoza Rivers, whereas annual minimal temperatures are around −7° C, occurring in June (Polanski, 1963). Precipitation does not exceed 200 mm per year. Violent summer storms cause large floods. The vegetation cover consists mainly of Andean steppe without trees. Because of aridity and strong evaporation, the drainage network is composed of both perennial and discontinuous rivers, which are occasionally supplied by storms. Perennial rivers originate in the high Frontal Cordillera where some glaciers are still in place.

Table 1. Correlation between the main paleo-climate cycles of the neighbouring areas. Data are taken from Harrison (2004); Clapperton (1983) and Espizua (1999, 2004)

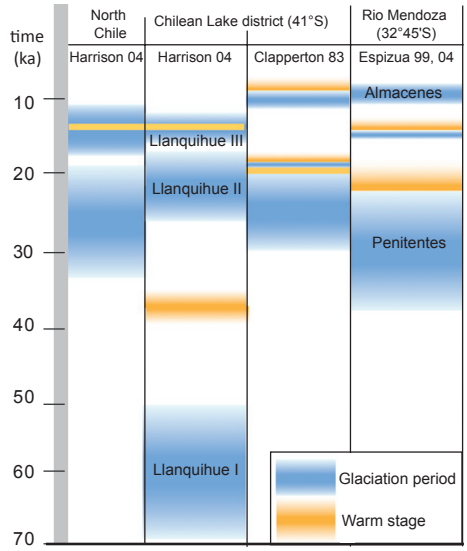

Paleo-climate proxies

The Late Pleistocene paleoclimate of the Las Tunas area is still not well known. Even though the climate is qualified by very local parameters such as rain and snow fall, altitude, humidity and temperature (Smith *et al.*, 2005; Condom *et al.*, 2007; Kull *et al.*, 2008; Zech *et al.*, 2008), we compiled several regional studies focused on the neighbouring areas to define a first-order approximation of the main glaciation cycles in the Las Tunas area (see Table 1). These studies are mainly based on cosmogenic nuclide dating and ^{14}C dating of moraines and river terraces. Three main warming stages have been described in the last 40 kyr. The most recent stage occurred ca.13–14 kyr ago that affected central Chile (Harrison, 2004) and the Mendoza River system located 100 km north of Las Tunas (Espizua, 1999, 2004). Another specific warming period corresponds to the end of the last glacial period that began ca.19–24 kyr ago south of 33° S. It followed the Penitentes Glaciation in Argentina (Espizua, 1999, 2004) and the Llanquihue II Glaciation in the Lake District of Chile (Clapperton, 1983; Harrison, 2004; Zech *et al.*, 2008). Finally, during the last glaciation a warm inter-stage occurred before 40 kyr that marks the end of the Llanquihue I glaciation in Chile (Harrison, 2004). Baker *et al.* (2009) found terrace incision periods that correspond to each of these past warming events in the Diamante River area located 100 km south of Las Tunas. In the piedmont region of Tupungato, Mehl and Zárate (2012) document a change from braided rivers from ca. 55 kyr to the early Holocene, to meandering rivers during the late Holocene. There is no well-constrained record of any older climatic transitions in the study region. However, a major glaciation was documented in northern Chile between 600 and 800 kyr (Harrison, 2004) and a sudden global change in the glacial-interglacial frequency occurred around 800 kyr (Pisias and Moore, 1981; Raymo *et al.*, 2006). Post-10 kyr, a warming stage has only been suggested, as moderated by Clapperton (1983) in the Lake District of Chile.

Geomorphological setting

Two main rivers, Las Tunas and Santa Clara, drain the 550 km^2 Las Tunas catchment. Their confluence

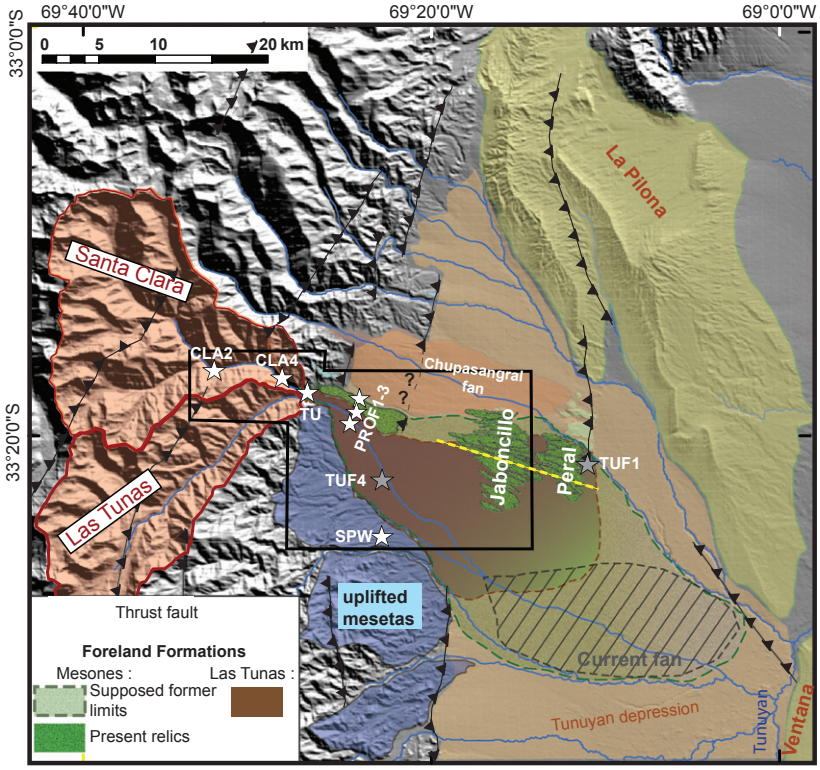

Fig. 2. The Las Tunas catchment-fan system. The mountainous section is composed of two subcatchments (in red). Foreland deposits consist of the Mesones Fm and the Las Tunas Fm. Stars indicate geochronological sample locations (see Table 2): PROF1-3 are pits for the ^{10}Be measurements in T1, T2 and T3, TU and SPW indicates the ^{10}Be surface samples TU1-TU2 and SPW1-SPW2 respectively. CLA2 and CLA4 are river sand samples; TUF4 and TUF1 are ash samples. The dashed yellow line across the Jaboncillo and Perral folds indicates the location of Fig. 3. The black box indicates the location of Fig. 8. To the east, La Pilona and Ventana are fault blocks of the piedmont.

is located at the mountain front (Fig. 2). Both drainage networks reach the high Frontal Cordillera. The southern Las Tunas drainage network also includes a volcanic area (Cerro Negro). The Las Tunas piedmont extends from the Cordillera front that forms its natural western and southern limit (see Fig. 2). The neighbouring Chupasangral fan and the Peral fold comprise the study area's natural northern and northeastern boundaries. The eastern limit of the Las Tunas piedmont is difficult to define because fans extend into the Tunuyán depression forming bajadas. The Ventana-Viscacheras block far to the east does not affect the Las Tunas fan.

Polanski (1963) was the first to describe the geology of this region. According to him, the piedmont is organized into two main units: the Las Tunas and the Mesones Formations (Fig. 2) that were later dated at between 30 and 200 kyr and 200 and 700 kyr old respectively. These ages were obtained from dated pyroclastic intercalations (i.e. Irigoyen *et al.*, 2002; García, 2004; Zárate and Mehl, 2008). García (2004) estimated the unit thicknesses in the piedmont (Tunuyán depression) using well data provided by Repsol-YPF, an oil and gas company, from near the Jaboncillo fold (Fig. 2). The maximum thickness of the Mesones Fm was evaluated to be ca. 100 m at the well site, whereas the Las Tunas Fm thickness can exceed 100 m. Analysing well data and compiling previous studies, García (2004) also provided a structural cross section of the major units (Fig. 3).

According to this study, Miocene deposits successively include the Mariño Fm (Middle Miocene) that might be linked to the deformation of the Principal Cordillera; the Higuerita ash, deposition of which is dated to have occurred between 12 and 11.5 Myr; the La Pilona Fm, which is estimated to be concomitant with the Cordon del Tigre uplift (Late Middle Miocene); the Angostura ash, dated around 9.3 Myr; and the Rio de los Pozos Fm. The main Pleistocene deposits include the Mesones and the

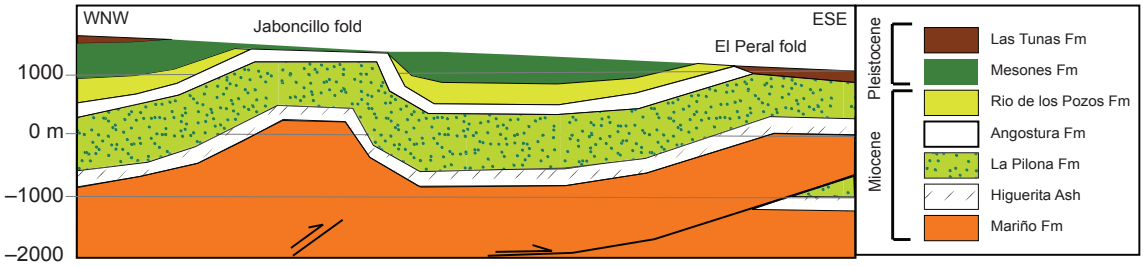

Fig. 3. Cross section showing the stratigraphy of the major units at the Jaboncillo and Peral folds according to García (2004).

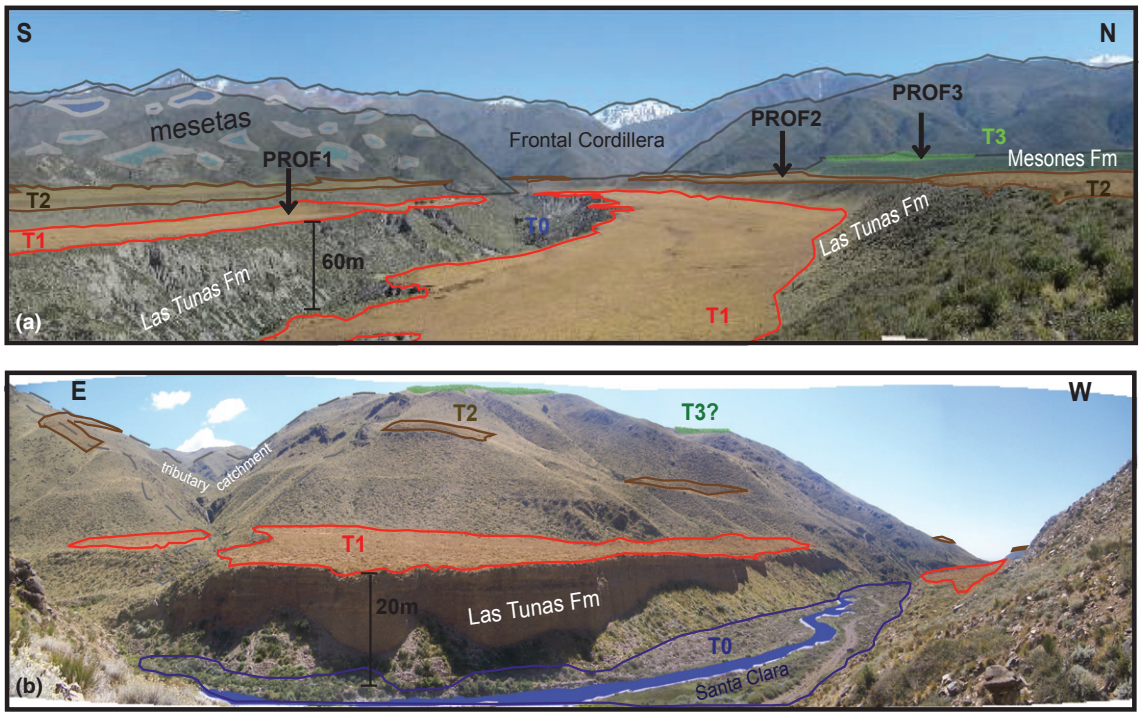

Fig. 4. (a) A view of the piedmont terraces. Black arrows indicate the TCN sampling pits. Blue polygons illustrate the uplifted surfaces named Mesetas. (b) Alluvial terraces in the mountain section. Photography locations are indicated in Fig. 8.

Las Tunas Formations. From this analysis, García (2004) linked an ash outcrop observed in the Peral fold with the Angostura Fm, but no chronological control is yet available to confirm this result. The Las Tunas catchment–fan system is characterized by well-preserved terrace levels. These terraces are recognized both in the mountain and in the piedmont, as illustrated in Fig. 4. The transition between mountain and piedmont has been defined in this study by the abrupt change of local slope in the catchment. In the piedmont, three main levels of terraces can be recognized. They are called *T*1 to *T*3 from the lowest to the highest respectively. *T*0 corresponds to the current river level (thalweg). The mountain river bed is alternately composed of alluvial sediment and bedrock. The piedmont river bed consists mainly of alluvial sediment. In the piedmont, T1, T2 and T3 are fill terraces whereas in the mountain part, fill and strath terraces alternate successively along the river main streams for at least both T1 and T2 levels. Locally at the transition from mountain to piedmont, T2 corresponds to a bedrock abrasion terrace.

METHODS

Landform analysis

We used digital elevation model (DEM) data extracted from the Shuttle Radar Topography Mission (SRTM) and from the Global Digital Elevation Map (GDEM) as well as 21 differential GPS profiles in the piedmont to reconstruct the three dimensional geometry of the Las Tunas system and build a detailed geomorphological map (see Fig. 5 for data locations). The vertical accuracy of the differential GPS data is around 10 cm, ensuring detailed mapping of the terrace geometry. The elevation of inaccessible surfaces was approximated using both GDEM and SRTM data. To ensure a good correlation in the mountainous catchment, DEM data were combined with hand-held barometric altimeter data, field observations and examination of 1 : 50,000 aerial photographs taken in 1966 by the 'Instituto Geografico Militar' of Argentina and ASTER images. Mountainous terraces are less preserved than those in the piedmont reach, mainly because erosion processes on steep adjacent hillslopes deposit material on their surfaces. Thus, mountain terraces are often not flat surfaces but present significant slopes normal to the river-flow direction. For this reason, the elevation of terraces in the mountains is less certain than that of piedmont terraces. The absolute vertical uncertainty of the DEM is estimated to be ca. 6 m for the SRTM (Farr *et al.*, 2007) and, according to its website, around 20 m for the GDEM. However, these uncertainties are not likely to cause piedmont to mountain terrace correlation errors given the large height difference between terraces (>>10 m) and the clear continuity of T1 and T2 observed in the field. To provide a general view of the terrace correlation, all of the longitudinal profiles of the terraces were projected along the active channel axis (Fig. 5).

^{10}Be Sampling sites

Two sand samples from the Santa Clara active stream were analysed (CLA2 and CLA4, Table 2, see Fig. 2 for location) to estimate the average erosion rate for the catchment. Even if this erosion rate (and thus sediment ^{10}Be concentration) may have changed through time, this concentration is useful as it indicates the magnitude of the ^{10}Be inheritance. These samples were collected from the river bed, to prevent additional inheritance due to sediment burial in terraces, at the catchment outlet and 10 km upstream.

Depth profiles were sampled on terraces T1 to T3 close to the proximal part of the piedmont and far from the deep canyon of the Las Tunas River. These sites show the best preservation of surfaces. For both the T1 and T3 profiles, a two metre deep hole was dug (see Fig. 6b). On T1, samples deeper than 3 m were collected from a fresh cliff scarp (Fig. 7d). The T2 profile was sampled by enlarging a fresh incision on a trail along the T2 surface. There is a deep sand lens at this location.

Samples from the T1 and T3 depth profiles consist of clusters of 1–7 cm granite pebbles (see Table 2). On T1, clusters are made up of more than 25 pebbles. On T3, quartz pebbles were less common, and so each sample consisted of ca. 15 clasts only. Samples of the last profile (T2) consisted of pockets of sand (ca. 0.5 kg) ensuring that each sample consists of thousands of individual clasts.

Two TCN surface samples (TU1 and TU2; Table 2, see TU in Fig. 8 for location) were collected from a quartz vein of a bedrock strath terrace correlated with the T2 surface. These surface samples are located at the mountain-piedmont transition (Fig. 9b), at the junction between the Las Tunas River and the Santa Clara River. At this location, paleo-beds of the river form stepped terraces incased within T2 (Figs. 6a,b and 9). These terraces indicate the migration of the Las Tunas River from the north-east section of the foreland to the south-west, probably at the early stage of the T2 abandonment process. By that time, the progressive lateral migration of the Santa Clara River eroded the rocky spur separating the two rivers at their junction, and then the Santa Clara River incised deeply into the bedrock, forming an epigenetic gorge apart from its previous paleo-canyon filled by sediment (Figs. 6a and 9b). This erosion process formed a bedrock strath terrace on gneissic rocks, where TU1 and TU2 were collected. The strath is horizontal over 10 m, not covered by sediment and cut into gneissic bedrock (Figs. 6a and b). TU1 and TU2 are samples of quartz veins on the strath surface taken 10 m apart. The strath terrace is about 5 m below the top of T2 (Fig. 6b). This ensures insignificant exposure (inheritance) before T2 entrenchment. The ^{10}Be concentration of TU1 and TU2 should allow the onset age of T2 incision to be determined.

The last two TCN surface samples consist of bedrock quartz (SPW1) and altered gravels (SPW2) from an uplifted meseta south of the Las Tunas system (Table

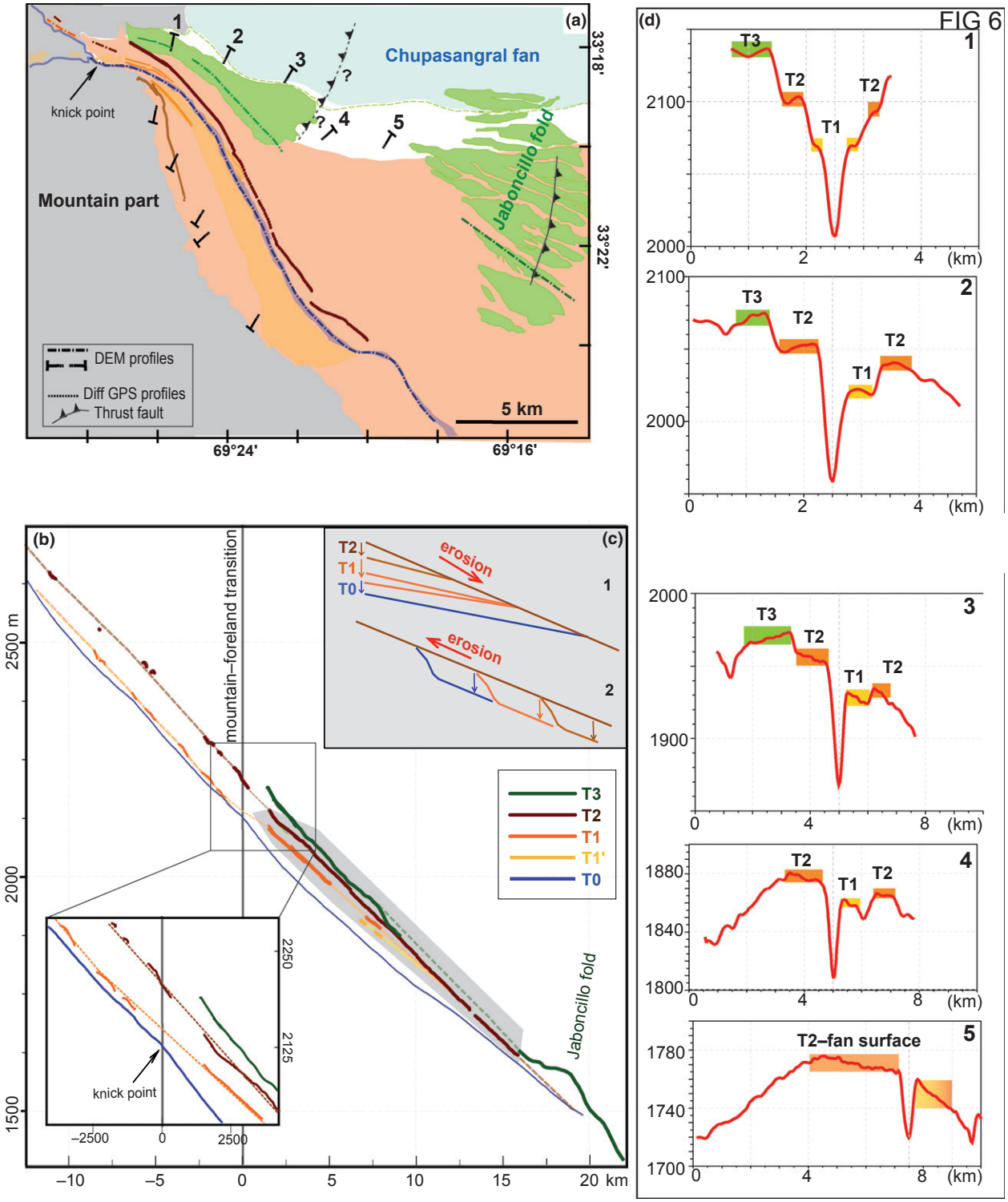

Fig. 5. (a) Location of the GPS (dotted) and DEM (dashed) longitudinal (colored) and transversal (in black) profiles. (b) Longitudinal profiles of the Las Tunas terraces. Note the vertical exaggeration. Dotted lines are interpretations. The grey area indicates the profiles with a vertical accuracy of ca. 0.1 m. Otherwise, it is ca. 10 m. (c) Schematic illustration of erosion wave propagation. In scenario 1, incision begins upstream and propagates downstream. The terraces are relicts of the successive river beds abandoned during the incision process. They converge downstream. In scenario 2, incision begins at the piedmont base (due to transverse river incision or piedmont uplift for instance) and propagates upstream. The terraces must intersect the original surface upstream in this case. The Las Tunas terraces geometry corresponds to scenario 1. (d) Transverse profiles of the Las Tunas piedmont created from DEM data. Green, orange and yellow colours highlight the T3, T2 and T1 locations respectively.

Table 2. Details of the geochronological samples, calculated ages and erosion rates

Sample name	Location	Description	Latitude (deg S)	Longitude (deg W)	Altitude (m)	Shielding correction	Depth (m)	Quantity	Production (at/g/yr)	[10Be] (10^5 at/g)	[10Be] error (10^5 at/g)	Calculated erosion rate ε and/or ages
PROF 1												
RIM 18	T1	pebbles: 3–7 cm	33.32	69.42	2048	0.997	0	19	17.3	3.31	0.39	
RIM 28	T1	pebbles: 3–7 cm	33.32	69.42	2048	0.997	0	>25	17.3	3.15	0.49	
RIM 20	T1	pebbles: 3–7 cm	33.32	69.42	2048	0.997	0.2	>25	17.3	1.73	0.22	acc. to exponential model:
RIM 22	T1	pebbles: 3–7 cm	33.32	69.42	2048	0.997	0.5	>25	17.3	2.12	0.37	
RIM 23	T1	pebbles: 3–7 cm	33.32	69.42	2048	0.997	0.7	>25	17.3	1.57	0.23	Abandonment age: 17–19 kyr
RIM 24	T1	pebbles: 3–7 cm	33.32	69.42	2048	0.997	0.9	>25	17.3	1.60	0.27	For ε = [0–10] m/Myr
RIM 27	T1	pebbles: 3–7 cm	33.32	69.42	2048	0.997	1.7	>>25	17.3	1.14	0.05	
RIM 15	T1	pebbles: 3–7 cm	33.32	69.42	2048	0.997	3.4	>25	17.3	0.62	0.03	
RIM 16	T1	pebbles: 3–7 cm	33.32	69.42	2048	0.997	3.8	>25	17.3	0.29	0.02	
PROF 2												
RIM 35	T2	sand	33.31	69.42	2070	1	0.1	3 kg	17.6	2.53	0.31	L1 (from 0 to 0.34 m deep): 11–20 kyr
RIM 36	T2	sand	33.31	69.42	2070	1	0.2	3 kg	17.6	2.51	0.45	for ε = [0–10] m/Myr and Co = [25–114] kat/g
RIM 37	T2	sand	33.31	69.42	2070	1	0.34	3 kg	17.6	2.47	0.37	
RIM 38	T2	sand	33.31	69.42	2070	1	0.5	3 kg	17.6	3.01	0.30	L2 exponential models: 10–31.6 kyr
RIM 39	T2	sand	33.31	69.42	2070	1	0.7	3 kg	17.6	2.95	0.19	for ε = [0–90] m/Myr
RIM 40	T2	sand	33.31	69.42	2070	1	0.91	3 kg	17.6	2.78	0.18	L2 mixing models: 60–45 kyr
RIM 43	T2	sand	33.31	69.42	2070	1	2.2	4 kg	17.6	2.42	0.10	for ε = [0–10] m/Myr and Co = [25–114] kat/g
TU 1	T2 fan apex	quartz from bedrock	33.30	69.46	2205	0.996	0	150 g	19.1	2.88	0.15	15.1 (± 0.8) kyr
TU 2	T2 fan apex	quartz from bedrock (10 m from TU1)	33.30	69.46	2205	0.996	0	750 g	19.1	3.94	0.13	20.7 (± 0.7) kyr
PROF 3												
RIM 5	T3	pebbles: 1–5 cm	33.31	69.41	2106	1	0.1	11	18	71.06	2.34	
RIM 6	T3	pebbles: 1–5 cm	33.31	69.41	2106	1	0.26	13	18	72.63	2.39	
RIM 8	T3	pebbles: 1–5 cm	33.31	69.41	2106	1	0.55	20	18	70.90	2.29	L1 (from 0 to 0.8 m deep):
RIM 9	T3	pebbles: 1–5 cm	33.31	69.41	2106	1	0.7	18	18	84.85	2.78	age > 0.85 Myr.
RIM 12	T3	pebbles: 5–8 cm	33.31	69.41	2106	1	1.03	2	18	45.11	1.52	acc. to mixing model

(Continued)

Table 2 (Continued)

Sample name	Location	Description	Latitude (deg S)	Longitude (deg W)	Altitude (m)	Shielding correction	Depth (m)	Quantity	Production (at/g/yr)	[10Be] (10^5 at/g)	[10Be] error (10^5 at/g)	Calculated erosion rate£ and/or ages
RIM 11	T3	pebbles: 1–5 cm	33.31	69.41	2106	1	1.3	8	18	45.70	1.66	
RIM 13	T3	pebbles: 1–10 cm	33.31	69.41	2106	1	1.55	17	18	40.74	1.39	
CLA 2	Sta Clara river (upstream)	sand	33.28	69.55	2498	1	0	4 kg	21.3	1.14	0.10	0.32 (± 0.06) mm/yr
CLA 4	Sta Clara river (downstream)	sand	33.29	69.48	2222	1	0	4 kg	20.3	1.22	0.14	0.28 (± 0.05) mm/yr
TUF 4	Las Tunas Fm	ash (amphibole)	33.36	69.38	1799							0.6 (± 0.2) Myr
TUF 1	Perral fold	ash (biotite)	33.36	69.18	1152							8.5 (± 0.2)Myr
SPW 2	mesetas	pebbles 0.2–1 cm	33.42	69.38	1755	1	0	>50	14.3	11.35	0.48	
SPW 1	mesetas	quartz from bedrock	33.42	69.38	1755	1	0	>500 g	14.3	18.58	0.56	

2, Fig. 2). The top of the mesetas consists mainly of a flat bedrock surface with some local sites presenting weathered rounded gravel. This flat surface was sampled for comparison with the T3 surface because weathered gravels present a similar facies at both sites, suggesting a similar surface abandonment age.

Sample preparation and analytical procedures

Samples were crushed and sieved at the Department of Geology at the Universidad de Chile into two uniform grain fractions ($0.25 < d < 0.5$ mm and $0.5 < d < 1$ mm). Magnetic grains were removed using a Franz magnetic separator. TCN depth profile sample preparation was carried out at Geosciences Environnement Toulouse (GET) using the procedure described by Von Blanckenburg *et al.* (1996), whereas surface and river sand samples were prepared at the Centre Européen de Recherche et d'Enseignement des Geosciences de l'Environnement (CEREGE) lab (Braucher *et al.*, 2011).

GET laboratory procedures begin with quartz separation using chemical leaching coupled with ultrasonic baths. Etching in a HF/HNO3 mixture removed several micrometres of the quartz grain surfaces and eliminated meteoric ^{10}Be. Be carrier (0.3 g of low noise carrier from A. Alimanovic, University of Melbourne, 1155 mg.L^{-1}, with $^{10}Be/^{9}Be$ <10) was added to ca. 20 g clean quartz samples that were subsequently dissolved in HF. Measured ^{10}Be ratios were corrected using process blanks treated in the same way as the samples. $^{10}Be/^{9}Be$ ratios in the samples were measured at the CEREGE ASTER AMS facility.

Calculation of ^{10}Be exposure age and mean erosion rates

Production rates were calculated using the CRONUS-Earth cosmogenic nuclide exposure age calculator (Balco *et al.*, 2008) using a modern sea-level and high-latitude ^{10}Be production rate in quartz of 4.5 at.g^{-1}.yr^{-1} (Stone, 2000). Ages were calculated using a ^{10}Be half-life of 1.36 Myr (Korschinek *et al.*, 2009; Chmeleff *et al.*, 2010). Scaling factors for topographic shielding were calculated using the surrounding topography of sampling sites and the CRONUS web calculator.

The ^{10}Be concentration of a sample C_{10Be} [at.g^{-1}] from a surface eroded at constant mean erosion rate ε [$g.cm^{-2}.yr^{-1}$] with time is given by (Siame *et al.*, 2000):

$$C_{10Be}(x,t) = C(x,0)\cdot e^{-\lambda t} + \sum \chi_i \cdot \frac{P_0}{\frac{\epsilon\rho}{\Lambda_i}+\lambda}\cdot e^{\frac{-\rho x}{\Lambda_i}} \cdot \left(1 - e^{-\left(\lambda+\frac{\epsilon\rho}{\Lambda_i}\right)t}\right) \quad (1)$$

In this equation, x (m) is the sample depth from the surface, t (yr) is the time during which the sample was exposed, $C(x,0)$ (at. g^{-1}) is the sample inheritance (i.e. the

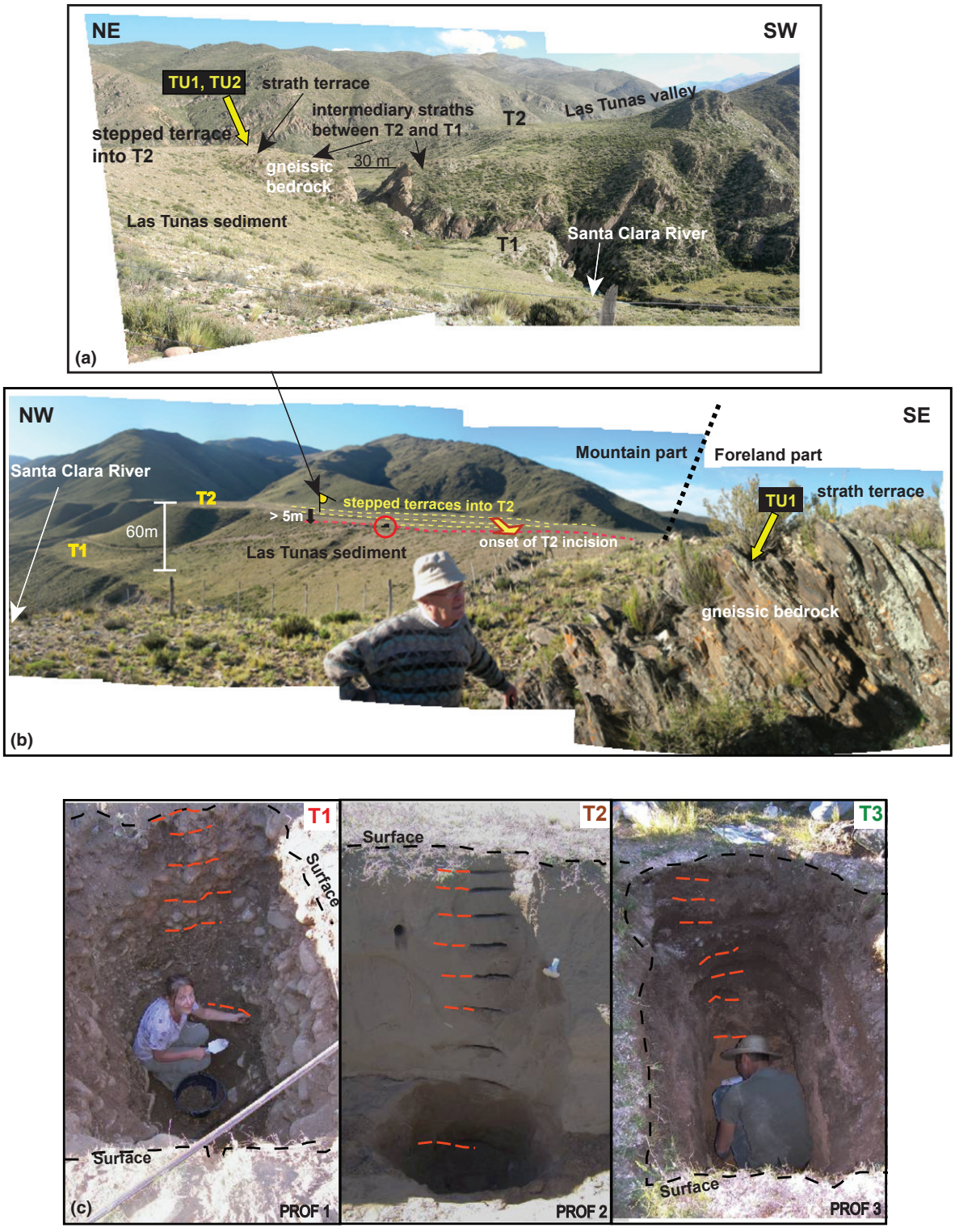

Fig. 6. Sampling sites. (a) View towards the SE showing the current entrenchment of the Santa Clara River near its junction with the Las Tunas River. Above, a strath terrace relict corresponds to a paleo-bed of this river. This relict correlates laterally to a stepped terrace slighly incased (5 m) within T2. Samples TU1 and TU2 were gathered at the surface of this strath terrace relict. (b) View towards the NE at near the junction between the Las Tunas and Santa Clara Rivers. Location of TU1 surface samples on the T2 apex. Stepped terraces incased within T2 are visible in the background and correspond to the markers of the Las Tunas River incision onset. TU1 and TU2 are located on the last paleo-bed occupied by the river before the major incision that led to abandonment of T2. Samples are from a bedrock strath. Note the car in the red circle providing a scale for the T2 subterrace incision. (c) Sampling pits for ^{10}Be concentration vs. depth profiles for T1, T2 and T3. Orange dotted lines indicate each sampling depth. See the locations of these photos in Fig. 8.

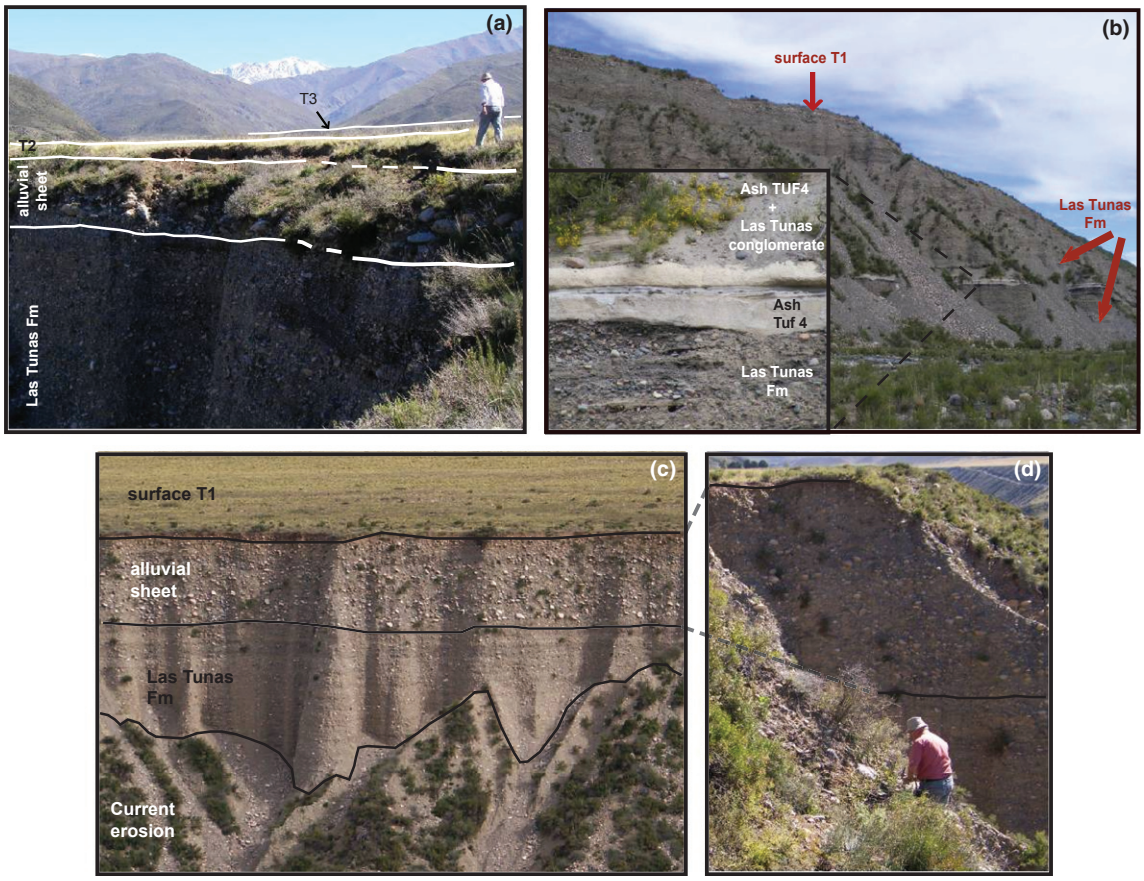

Fig. 7. (a) Below the T2 surface, a 2–3 metre thick layer that forms the T2 alluvial sheet is deposited on the Las Tunas Formation. (b) Ash flow interbedded in the Las Tunas Fm and TUF4 sample location. (c) and (d) The succession of the Las Tunas Fm and more recent alluvial sheet strata under the T1 surface. The locations of photographs b and c are indicated in Fig. 8.

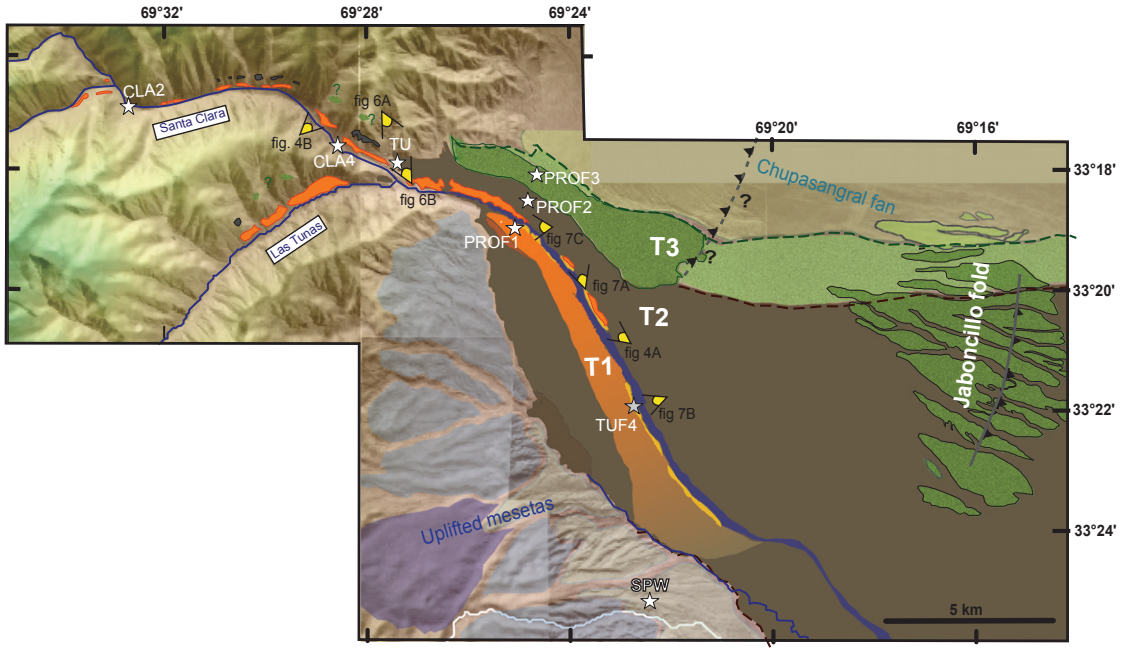

Fig. 8. Geomorphological organization of the Las Tunas System. Mesones Fm deposits are in green (the light green colour corresponds to the assumed former Mesones extent). The extent of the Las Tunas Fm corresponds to the T2 and T1 areas. In the piedmont, the brown (orange) color indicates the current T2 (T1) alluvial sheets above Las Tunas Fm. Both assumed former deposit boundaries are indicated in colored dotted lines. The stars indicate the geochronological sample locations (see Fig. 2 for details). Eye symbols indicate the photography locations from Figs. 4, 6, 7.

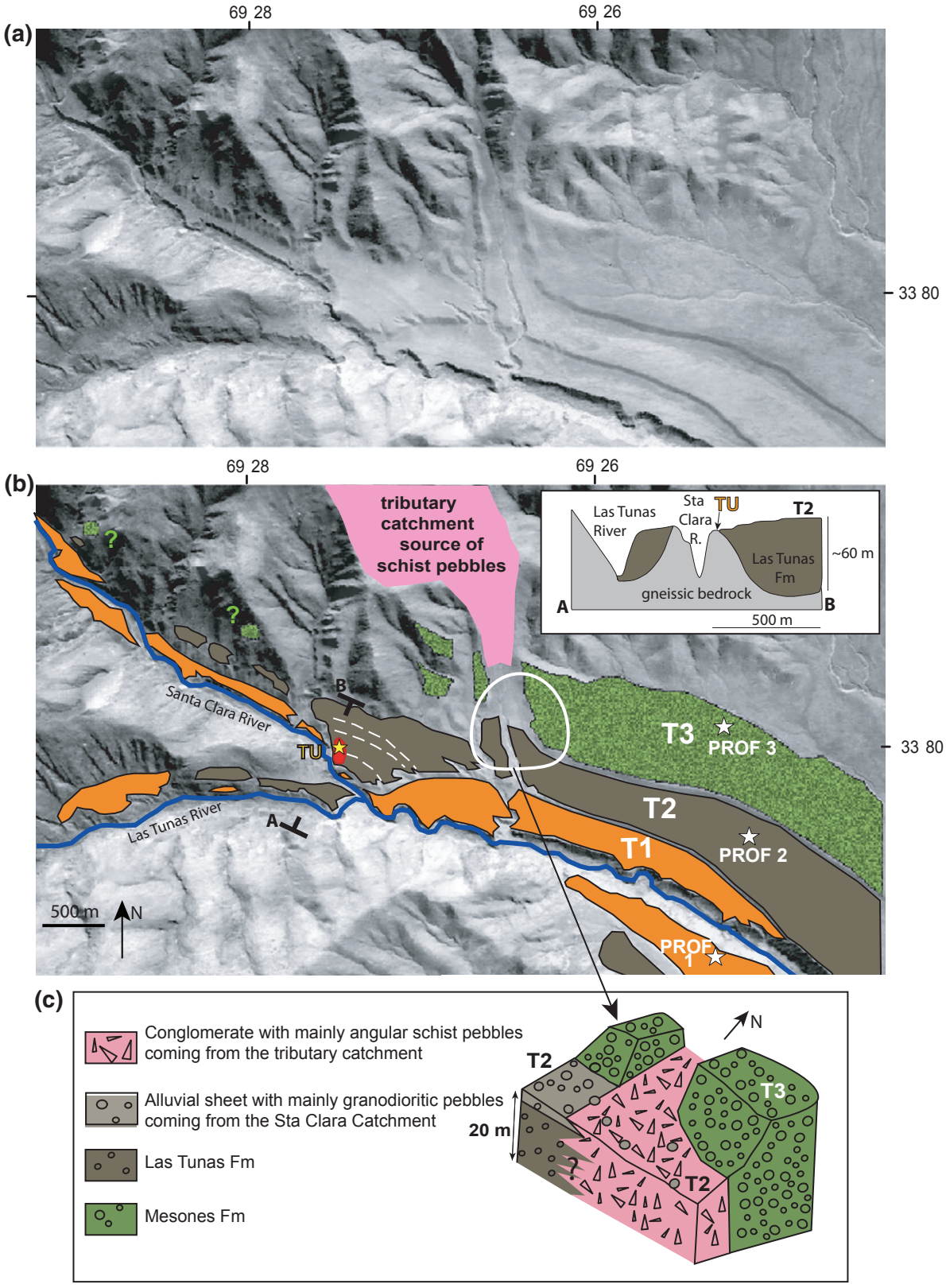

Fig. 9. (a) Aerial photograph of the Las Tunas mountain to piedmont transition. (b) Geomorphological map of the mountain to piedmont transition. The apex of T2 in the piedmont is characterized by several sublevels illustrated by dashed white lines. On the lowest level, a strath terrace relic is visible (in red) and marks the last river level before its deep incision within gneissic bedrock. The inset AB section shows that the Santa Clara River eroded laterally and incised itself within the rocky spur that separated the Santa Clara and Las Tunas Rivers before the Santa Clara River entrenchment. Samples TU1 and TU2 are taken on this strath relict (see also Figs. 6a and b). T1 and T2 are correlated from piedmont to mountain using their relative elevation in cross section and along stream. (c) 3D Schematic representation of the T2 and T3 infills in front of the small tributary catchment (in pink on B) that locally provided schist pebbles.

sample ^{10}Be concentration at the initiation of the present surface exposure episode), λ is the radioactive decay constant (4.610^{-7} yr^{-1}), χ_i are the relative contributions of neutrons, slow and fast muons to the total surface production rate, (0.98, 0.02 and 0.01 respectively; Braucher *et al.*, 2003), $P0$ ($at.g^{-1}.yr^{-1}$) is the surface production rate, ρ the rock density (2.5 g cm^{-3}) and Λ_i the corresponding attenuation coefficient (150, 1500 and 5300 g cm^{-2} respectively).

Clusters of grains were sampled at different depths x at three sites using the method established by Anderson *et al.* (1996) and Braucher *et al.* (2009). When the TCN concentration vs. depth profiles fit an exponential curve, we determine the optimum values of t and ε by calculating a minimum χ^2 value using the procedure of Siame *et al.* (2004); Ritz *et al.* (2006) and Braucher *et al.* (2009). This procedure allows us to plot the confidence region of the solution at 68% (1 σ) in the (erosion rate, exposure time) matrix taking into account each sample of the profile.

For profiles that show a constant $C_{^{10}Be}(x)$ with depth, we use a mixing model that evaluates the mean concentration value representative of the entire mixed layer to provide an approximation of the time during which the layer under consideration was mixed (see Appendix). The exposure ages of the surface samples were evaluated using Eqn (1) and the assumptions on the erosion and inheritance parameters justified by geomorphological observations (see Braucher *et al.*, 2009, and the Results and Discussion sections of this study for details).

The concentration of ^{10}Be, $< C_{^{10}Be} >$, of river sand samples allows us to estimate the mean erosion rate $<\varepsilon>$ in the catchment upstream from the sampling site. The mean erosion rate was calculated using (e.g. Brown *et al.*, 1995; Granger *et al.*, 1996):

$$\langle \epsilon \rangle = \sum \chi_i \frac{\Lambda_i}{\rho} \cdot \left[\frac{\langle P_0 \rangle}{\langle C_{^{10}Be} \rangle} - \lambda \right] \quad (2)$$

This model assumes that the mean $C_{^{10}Be}$ is stationary on the hillslope and its accumulation during river transport is zero. The mean production rate $\langle P_0 \rangle$ is averaged over the catchment area. The local production rate of each SRTM pixel of the catchment is calculated as a function of the elevation using the scaling laws of Stone (2000), and taking into account the topographic shielding (Codilean, 2006).

$^{40}Ar/^{39}Ar$ dating

To constrain the timing of sediment deposition, we obtained $^{40}Ar/^{39}Ar$ dates for two of the ash layers interbedded within the piedmont sediment deposits. One layer is interbedded within the Las Tunas Fm gravels below the T1 surface (see Table 2- TUF4 for details, Figs. 2 and 7 for location). The second layer, where sample TUF1 comes from, is located in an outcrop of the Peral fold and is between 2 and 10 m thick (see Table 2- TUF1 and Fig. 2). The Peral outcrop is composed of alternating sands and conglomerates. It is stratigraphically below the sedimentary layer visible on the flank of the Jaboncillo fold that we assume to be the Mesones Fm.

The $^{40}Ar/^{39}Ar$ geochemical analysis of both TUF4 and TUF1 was carried out at the laboratory of SERNAGEOMIN (SErvicio NAcional de GEología y MIneria of Chile). They consisted of step heating plateau ages and isochrons on biotite (TUF1) and amphibole (TUF4). The plateau seems well defined in both cases and no Argon excess was detected for both samples, indicating that the $^{40}Ar/^{39}Ar$ analysis provided ash deposition ages.

RESULTS

Terrace morphology

In the piedmont, the highest (T3) terrace abruptly ends 7 km downstream from the mountain front (Figs. 5 and 8). Thus, we suspected an offset produced by faulting in the mountain front north of T3 had propagated through the Chupasangral fan and the T3 front (Fig. 2). However, we were not able to observe any direct faulting features. In the Santa Clara and Las Tunas mountain catchments, old surfaces are visible that could correspond to T3 remnants, but they are too strongly eroded to allow reliable correlations (Fig. 8).

T1 and T2 surfaces extend continuously from piedmont to mountain. This continuity is observed on longitudinal profiles (Fig. 5) and in plan view at the mountain to piedmont transition (Figs. 4 and 9).

Both the T1 and T2 surfaces extend upstream from the piedmont to 10 km in the mountain catchment. There, both terraces are cut by tributaries (see Fig. 8). In the piedmont, T2 is continuous on both sides of the Las Tunas valley. On the other hand, T1 extends mainly on the southern side and is cut and discontinuous on the northern side of the Las Tunas River. Transverse profiles provide additional information about the piedmont terrace organization (Fig. 5d). T2 and T1 have an increasingly convex shape from the mountain front downstream. This suggests that both surfaces correspond to an alluvial fan structure. Thus, after the incision of the T2-fan, the T1 fan structure has been built and then strongly incised.

In the piedmont, T3 lies 20 m higher than and parallel to T2. In contrast, T0, T1 and T2 converge downstream (Fig. 5b). The projected convergence point of T2 and T1 is located ca. 12 km from the mountain front, followed downstream by the convergence point of T1 and the current Las Tunas River T0 level at ca. 20 km. Downstream from this junction, the Las Tunas piedmont is composed of a single surface that extends into the Tunuyán depression forming bajadas. The maximum elevation difference between each level is reached at the mountain front. At this location, T1 is ca. 70 m above T0, T2 is ca. 35 m above T1 and T3 is 20 m above T2. In the piedmont,

maximal incision since T3 and T2 abandonment is thus ca. 125 m and 105 m respectively.

In the mountain range, both T1 and T2 terraces are parallel to the T0 level. T2 is around 100 m above T0 (equivalent to the value at the piedmont apex). T1 lies 20 m above T0 in the mountain, making it 50 m lower than at the piedmont apex. This geometry implies that the post-T1 incision was much more significant in the piedmont than in the mountain valley (Fig. 5b). The presence of bedrock 20 m below the T1 surface in various locations along the mountainous T0 level could be responsible for such a contrast in incision. Although incision becomes more difficult in the mountain range when river incision reaches bedrock, the piedmont remains easily erodible because of the softer sediment infill.

Terrace sedimentology

No fresh T3 fill section exists in the landscape, but we observed the T3 surface deposits in the piedmont when sampling the TCN profile of T3. The upper 2 m of T3 does not present stratification. They are made of isolated weathered granodioritic pebbles from centimetric to decimetric size mixed with a uniform sandy matrix. These weathered sediments are also visible on the flank of the Jaboncillo fold and correspond to the Mesones Fm (Polanski, 1963).

In the piedmont, the sedimentology of deposits topped with T1 and T2 terraces suggest that they correspond to the Las Tunas Fm described by Polanski (1963). These deposits are crudely horizontally bedded, sandy matrix supported, with mainly granitic rounded pebbles in the range of several centimetres to 10 cm (Figs. 6 and 7). The beds contain different proportions of pebbles. We did not observe paleo-soils in these deposits. The thickness of this alluvial unit is at least 60–100 m, which corresponds to the Las Tunas river incision below T2 (Figs. 4 and 5). This formation is covered by a crudely to not stratified alluvial sheet, composed of unimbricated rounded clasts supported by a sandy matrix (see Figs. 7a and c). In average, these clasts are bigger than in the Las Tunas Fm. Their larger length reaches around 30 cm, which constitutes the only property that allows these younger units to be differentiated from the underlying Las Tunas Fm. We estimated that the alluvial sheet of T2 is ca. 2 m thick and that of T1 reaches a thickness of 4–5 m near the fan apex (Fig. 7).

These alluvial sheets characterize the last depositional event before abandonment of their respective terraces. On both the T1 and T2 surfaces, we observed fluvial paleo-bars and paleo-river braided features that are around 50 cm high. These remnants suggest that erosion has been weak on these surfaces since their abandonment.

At isolated T2 surface sites near the piedmont apex, a fine, several metre thick sandy deposit is visible (see the T2 ^{10}Be sampling site for an example, Fig. 6b). Polanski (1963) and Zárate (2002) described it as the El Zampal Fm with an eolian origin. However, because of its discrete location, its absence on the other terraces (especially on the oldest T3 surface) and the presence of scattered centimetre-sized pebbles in the sediment, we assume it is the final river deposit at the end of a sedimentation period on T2. We interpreted this deposit as an alluvial lens.

As illustrated by Fig. 9, near the mountain-piedmont transition, the infill below T2 is mainly composed of angular schist pebbles, contrasting with the upstream part of T2 where the deposit is mainly constituted of granodioritic pebbles sourced in the Las Tunas and Santa Clara catchments. The angular schist clasts come from a small tributary catchment (see location in Fig. 8). This tributary has deeply entrenched the T3 surface. On the flanks of this incision, the lithology of T3 is mainly composed of rounded granodioritic pebbles, typical of the Mesones Fm. A recent incision perpendicular to the T2 terrace flank allows the schist pebbles to be observed to at least 20 m deep within the T2 infill. The portion dominated by schist clasts can be interpreted as a lateral alluvial fan inserted within the Santa Clara sediment constituting the Las Tunas Fm (Fig. 9c). This configuration indicates that the Mesones Fm (topped by T3) was deeply incised before the Las Tunas Fm infill.

In the mountain range, only the fill terraces correlated to the T1 level by morphological analysis have fresh scarps (see Fig. 4). The lithological composition and structure of these alluvial terraces are similar to the Las Tunas Fm (crudely stratified, sandy matrix and unimbricated granitoid pebbles smaller than 10 cm). Thus, we associate this infill with the Las Tunas Fm as suggested previously by Polanski (1963). However, the superficial alluvial sheet developed above the Las Tunas Fm on T1 in the piedmont is not visible in the mountain range. Thus, the final agradational process that allowed the development of these final deposits seems to only have affected the piedmont. The alluvial stratigraphy of terraces correlated to the T2 level in the mountain is less clear than for T1, because T2 surfaces present eroded and vegetated flanks (see Fig. 4). However, in some locations, tributary catchments have strongly entrenched the terraces to reach the Santa Clara River. These places allow us to observe rounded centimetre-sized granitic pebbles in conglomerate similar to the Las Tunas Fm on T2 flanks in the piedmont.

Finally, the presence of alluvial sediments along T0 and the uniformity of the T2 elevation above T0 from piedmont to mountain indicates that the T2 surface was built on a sediment infill that was at least 100 m thick in both the mountain range and the piedmont. This argument is re-enforced by the absence of a visible strath or bedrock surface in any of the lateral incisions affecting the flanks of T2 and T1 on the piedmont. These results exceed the previously measured thickness of the Las Tunas Fm at the Peral fold (García, 2004).

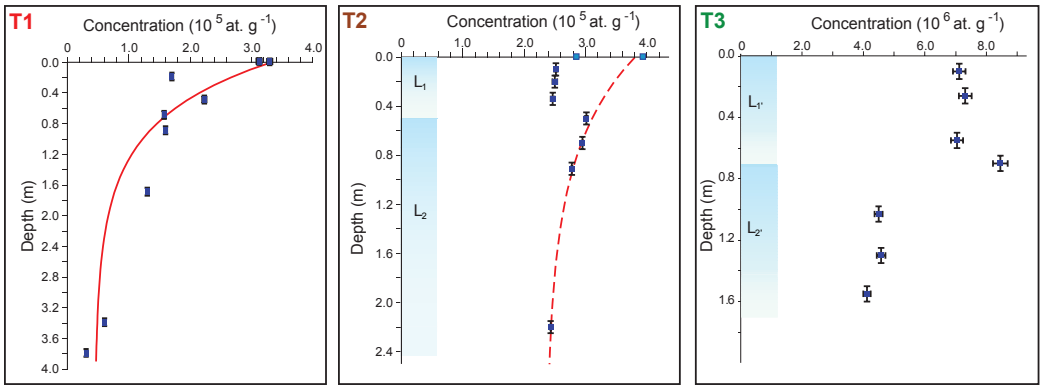

Fig. 10. ^{10}Be Concentration vs. depth profiles for T1, T2 and T3. Layers identified in the T2 and T3 terraces are indicated on the left. Note the different ranges for each axis scale. Theoretical exponential profiles are in red. Dotted red profile for T2 represents theoretical profile taking only the second layer into account.

$^{40}Ar/^{39}Ar$ dating of the volcanic ash

TUF4 step heating plateau ages are 0.5 ± 0.2 Myr (see Appendix, Fig. A) and the isochron analysis gives an age of 0.7 ± 0.4 Myr. Therefore, we determined the age of TUF4 to be ca. 0.6 ± 0.4 Myr. As this ash is interbedded in the Las Tunas Fm, the deposition of this unit took place 0.6 Myr ago.

TUF1 step heating on biotite gives a plateau age of 8.7 ± 0.2 Myr and the isochron age is 8.3 ± 0.15 Myr. This ash thus corresponds to the Angostura Fm described by Polanski (1963) and is dated at between 9.5 and 8.4 Myr by Irigoyen *et al.* (2002) using an $^{40}Ar/^{39}Ar$ analysis on biotite. These results support the stratigraphic description of García (2004) and agree with Polanski (1963).

^{10}Be analysis

River sand and mean catchment erosion rate

The two river samples CLA2 and CLA4 have similar $[^{10}Be]$ values of 1.14 10^5 and 1.22 10^5 at.g^{-1}. Using Eqn (2), river sand samples CLA2 and CLA4 values yield mean erosion rates of ca. 0.30 ± 0.06 mm.yr^{-1} for the Santa Clara catchment. The uncertainty is the propagation of the analytical errors and a ±10% uncertainty assumed on the production rates within the catchment.

Geomorphic markers

TCN depth vs. concentration profiles are illustrated in Fig. 10. In the case of T1 and T2, the sampling at depth was limited to the alluvial sheet covering the Las Tunas Fm, to avoid mixing sediment with potentially different exposure ages, and to date the last sedimentation event before surface abandonment.

The T1 profile presents a maximum ^{10}Be concentration at the surface. Concentrations decrease exponentially with depth. However, dispersion around this exponential feature is significant, suggesting that more than 25 clasts per depth are necessary to obtain a better average estimate of inheritance at each depth (i.e. Anderson *et al.*, 1996).

The two surface samples from the T2 strath have ^{10}Be concentrations of around 2.9 10^5 at.g^{-1} for TU1 and 3.9 10^5 at.g^{-1} for TU2.

The ^{10}Be concentration vs. depth profile for T2 is composed of two layers (L_1 and L_2 in Fig. 10). The first layer, between 0 and 0.5 m depth, has a uniform ^{10}Be concentration. The second, extending from 0.5 to 2.2 m, presents higher ^{10}Be concentrations and a gentle decrease of concentration with depth. We interpret the pattern of this profile as the mixing of clasts within the superficial alluvial sheet of T2.

Similar to T2, T3 does not have an exponentially decreasing concentration with depth, but is composed of two layers: $L_{1'}$ from 0 to ca. 0.8 m depth and $L_{2'}$ from 0.8 to at least 1.55 m depth. Each layer has a relatively constant concentration value with some scattering. Part of the dispersion is due to the small numbers of clasts in each sample, biasing the ^{10}Be concentration average at each depth.

The two surface samples collected on the uplifted meseta south of Las Tunas have ^{10}Be Concentrations of around 18.6 10^5 at.g^{-1} for the bedrock sample (SPW1) and 11.3 10^5 at.g^{-1} for the gravel cluster (SPW2) These concentrations are much lower than the concentrations determined at the surface of T3. Thus, the two surfaces cannot be correlated.

Estimating exposure ages and erosion rates

T1 abandonment

Assuming a mean inheritance of T1 clasts of 25 000 at.g^{-1}, similar to the deepest sample concentrations, the best-fit age deduced from a minimum χ^2 value is 30 ±10 kyr and the best fit erosion rate ε is 36 ± 15 m.Myr^{-1} (Fig. 11). These results infer the erosion of the T1 surface to be ranging between 0.4 and 2 m since its abandonment. The paleo-bars and paleo-river braided features observed on

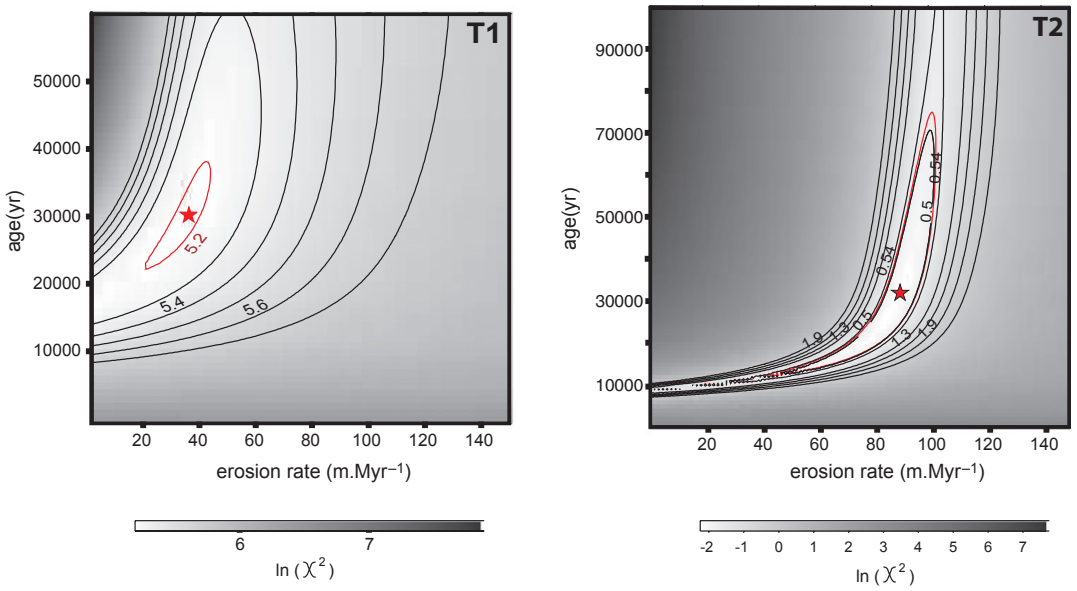

Fig. 11. χ^2 diagram for T1 and T2 exponential profiles using the method of Siame *et al.* (2004). Contours indicate $ln(\chi^2)$ isovalues. Stars indicate the best couple (t,ε), red lines indicate the value at 1σ.

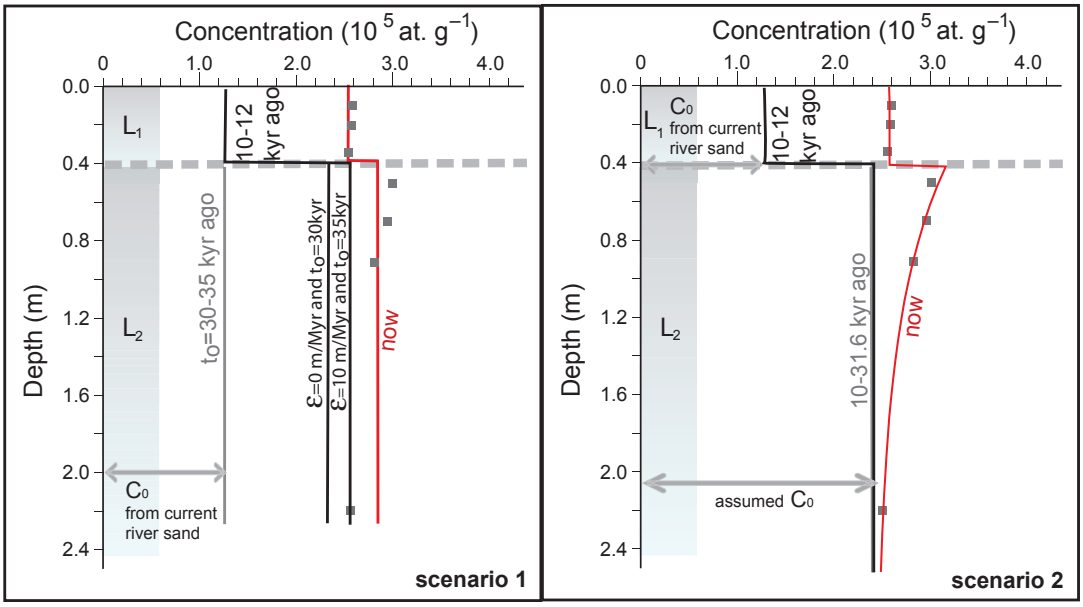

Fig. 12. Two possible models of the T2 ^{10}Be profile evolution. Measured ^{10}Be concentrations are in grey squares. Lines indicate the profile evolution through time until now (red line). In both scenarios, the paleo-surface in dashed grey shows the top of the L_2 layer before the deposition of L_1. Inheritance is assumed to be the current river ^{10}Be concentration. The erosion rate is assumed to range between 0 and 10 m Myr^{-1}. In scenario 1, L_2 has been mixed continuously for the last 30–35 kyr and L_1 for the last 11–12 kyr. In scenario 2, the ^{10}Be concentrations of L_2 develop an exponential depth-profile from a depth constant inheritance and after the deposition of L_1. The model profile fits the data for a L_2 burial age of 8–11 kyr, which is consistent with a mixing age of L_1 of 11–12 kyr in both scenarios. With smaller initial inheritance equal to that of T1 profile (25000 atg^{-1}) and for the same erosion rate range, the mixing of L_2 has occurred for the last 45–60 kyr in scenario 1 and the mixing of L_1 lasted 17–20 kyr in both scenarios (not illustrated).

T1 suggest that this is an overestimate of the amount of erosion that has occurred, and therefore that the age of T1 is probably less than 30 kyr. A range of ε from 0 to 10 m.Myr^{-1} has been tested, based on their use as bounding values by Baker *et al.* (2009) for the terraces of the neighbouring Diamante River. With such a range of ε, the model age of T1 ranges between 17 and 19 kyr. Baker *et al.* (2009) estimated a lower mean erosion rate of 1.3 m.Myr^{-1} for a disconnected terrace remnant.

Abandonment of the bedrock relict correlated with the T2 apex

Because of the planar morphology and the gneissic nature of the sampled strath relict, we estimated that its erosion rate is insignificant. Inheritance was assumed to be null as discussed above (see the ^{10}Be sampling site section). According to these hypotheses, abandonment of the T2 surface at its apex due to incision can be evaluated to be around 15.1 ± 0.8 kyr using TU1 and around 20.7 ± 0.7 kyr using TU2 (errors correspond to the internal uncertainty 1 σ of ^{10}Be measurements). An erosion rate of 10 m.Myr^{-1} would change the central values to 17 kyr for TU1 and 25 kyr for TU2.

Abandonment of T2 alluvial surface

^{10}Be concentrations within the layers L_2 are high and show little variations with depth. Considering either that these variations are not significant or that they are significant, two different scenarios for the T2 alluvial sheet (Fig. 12) are discussed in the following paragraphs. In both scenarios, L_1 is deposited after L_2 because L_1 has a lower mean ^{10}Be concentration than L_2.

In the first scenario, we assume that the ^{10}Be concentrations within L_2 are not significantly different, and thus that L_2 has been mixed continuously up to now. The superficial L_1 layer was deposited and has been mixed above L_2. The surface was eroding at a constant rate during all the process. The erosion rate is assumed to range between 0 and 10 m.Myr^{-1} as in case of T1. A mixing model is used to estimate the mixing duration of both layers (see Appendix). Inheritance is first approximated using the value of our current river sand samples (CLA2 and CLA4). Using these parameters, L_2 mixing has occurred for the last ca. 35 to 30 kyr according to the tested erosion rate. The superficial L_1 layer has been deposited and mixed for the last ca. 11–12 kyr for the same erosion rate range (Fig. 12). If we assume a lower inheritance, equal to the inheritance used for T1 (25 000 at.g^{-1}), then L_2 has been mixed for the last 60 to 47 kyr and L_1 for the last 17–20 kyr.

The second scenario considers the exponential trend in L_2 as significant. In this scenario, the ^{10}Be concentration of L_2 evolves from a depth constant value (ca. 2.3E-5 at.g^{-1}). This value may correspond either to a pre-deposition ^{10}Be concentration of fluvial sediment, or to the mean ^{10}Be concentration resulting from some period of mixing before the deposition of L_1. In the first case, a mean paleo-erosion rate of the mountain catchment source Eqn (2) can be estimated at ca. 0.16 ± 0.03 mm.yr^{-1}. In the second case, using the same erosion rate range and inheritance value as in scenario 1, the depth constant value ca. 2.3E-5 at.g^{-1} results from a mixing period that lasted 20–25 kyr before the deposition of L_1, 12 to 11 kyr ago. Assuming a lower inheritance equal to that of T1, the mixing of L_2 lasted 23–27 kyr before L_1 deposition.

Then, L_2 is buried by L_1 and an exponential depth-^{10}Be concentration profile develops. The L_2 burial age can thus be determined by fitting its ^{10}Be concentration profile using Eqn 1 (Fig. 10). Using the inheritance value 2.3E-5 at.g^{-1}, the best fit burial age of L_2 is 31.6 kyr for ε = 90.6 m.Myr^{-1} (Fig. 11b). Both values seem overestimated. They imply an erosion of 2.7 m which seems unlikely given that some ancient bars and an interbedded paleo-channel are still visible close to the sampling location. For ε ranging between 0 and 10 m.Myr^{-1}, the burial age of L_2 ranges between 8 and 11 kyr (Fig. 11b).

To summarize, the last deposition event on T2 corresponds to L_1 and is dated between ~11 kyr and 20 kyr depending on the considered erosion rate and inheritance value. The meaning of the high ^{10}Be concentration of the deepest sample of L_2 remains ambiguous. If it corresponds to a period of mixing, this period ranges between 60 to 11 kyr ago depending on the erosion rate and inheritance. This mixing could be due to Las Tunas River avulsions on the T2 surface and/or by efficient bioturbation. This period may correspond to a major aggradation event proposed by Baker *et al.* (2009) (c.f. their QT3 terrace building) and by Mehl and Zárate (2012) 40 km downstream.

Abandonment of the T3 alluvial surface

The high ^{10}Be concentration in the deep levels and the strong weathering of the pebbles observed in the soil pit suggest that T3 is an old surface. The mean ^{10}Be concentration at 1.5 m depth is 30 times larger than the concentration measured in the current Las Tunas River, suggesting that inheritance can be neglected. In the absence of independent data for the T3 erosion rate, we calculate the minimum ages assuming a zero surface erosion rate.

The mixing concentration method on L_1 suggests that this layer was in place and mixed since at least 0.85 Myr. Thus, T3 would be very much older than the T1 and T2 surfaces and dates back to the early Pleistocene.

DISCUSSON

Subsurface mixing

Our TCN profiles show strong remobilizations affecting the top 0.5–2 m of both the young (and sandy at the sampling site) T2 and the old pebbly conglomeratic T3 surfaces. Both surfaces are very planar and disconnected from the drainage network, which makes the remobilization process intriguing. Analysis of the T2 alluvial sheet suggests that its deep layer L_2 could have been mixed by the fan deposition processes, including avulsions and lateral movements of the flow suggesting that the river had a stable long profile at the T2 eleva-

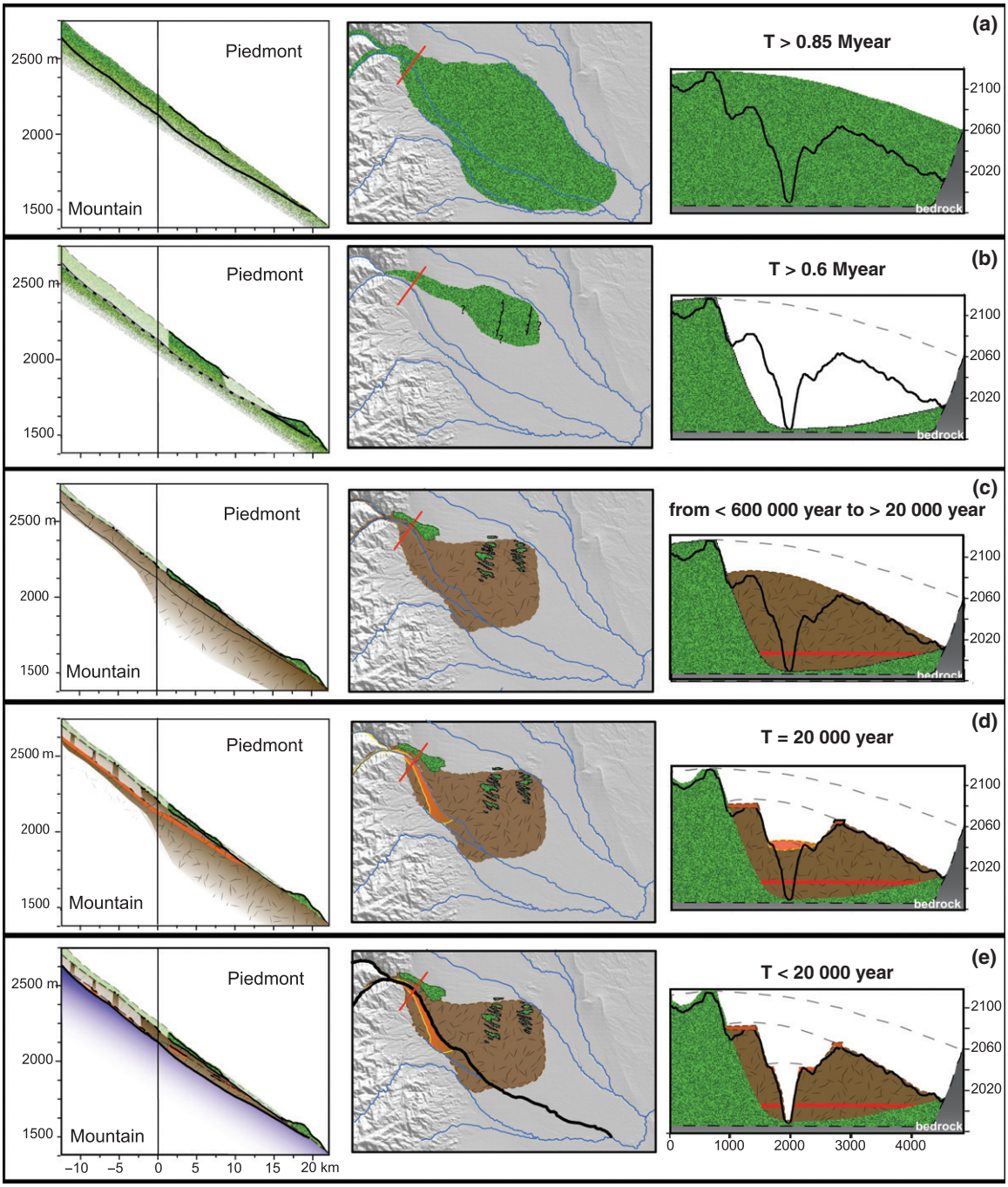

Fig. 13. Schematic evolution of the Las Tunas landscape over time. The left column illustrates a longitudinal transect along the main river. The middle column shows a map view; the right column represents a transverse transect (location is indicated by the red line on the map). (a) Deposition of the Mesones Fm (green) is followed by major incision. (b) Mesones Fm is thus preserved only in a few locations such as the Jaboncillo fold. The Las Tunas Fm deposition (brown) followed. (c) Note the interbedded TUF4 ash illustrated by orange line on the transverse transect. It is followed by two erosion periods that lead to T2 and T1 formation and incision (d and e).

tion for a significant duration. However, this process cannot explain the mixing of the surface layer L_1, which has been remobilized after deep incision and abandonment of the T2 surface. Remobilization in T3 cannot be easily explained.

The mixing process could have been bioturbation, as suggested previously by Heimsath *et al.* (2002) who carried out a numerical modelling study of flat surface mixing. However, the mixing of decimetric pebbles by bioturbation processes appears difficult to explain. Mixing might also be the consequence of unchannelized surface erosion such as successive sheet flow episodes, as suggested elsewhere (Perg *et al.*, 2001; Bierman *et al.*, 2001; Le Dortz *et al.*, 2011). Violent summer

storms might have supplied transient floods on the flat surfaces and transported some sediments on the gentle slope of surfaces. If we assume that such occasional flooding has occurred for the last 20 kyr, extreme events could be responsible for transient pebbles transport and surface remobilization. In this case, paleo-bars on the T1 and T2 surfaces might be markers of the transient flows.

The possibility that the T2 surface could have been affected by post-incision sediment deposition and the mixing of material from the T3 terrace walls in the piedmont is unlikely. In the proximal region of T2, this surface dips gently toward T3 (see transverse profiles 1 and 2 in Fig. 5), with a gully in between, preventing any deposition of T3 material at the location of the soil pit dig in T2.

A period of intense vegetation cover on the piedmont might have significantly enhanced the surface mixing of T2 and T3, but no evidence of such vegetation (e.g. buried wood, carbon material) was found during TCN sampling.

Finally, soil creep and fine sediment remobilization by seasonal climatic conditions could be involved in the surface mixing processes. Our results show that even if the mixing of abandoned surfaces is not visible in the field, this process can be efficient. If this occurs, samples gathered at the surface could have experienced a complex burial and exposure history after surface abandonment. In this case, their cosmogenic nuclide concentration underestimates the exposure age if the mixing is not taken into account in the age calculation. A mixing model yields a better estimation of the surface age.

Chronology of landscape development at Las Tunas

Figure 13 provides a chronological interpretation of the Las Tunas landscape history based on our geomorphological and geochronological analysis. The T3 surface layer was mixed by 0.85 Myr at the latest. Thus, the Mesones Fm, on which the T3 surface is developed, was deposited in the Las Tunas piedmont before 0.85 Myr (Fig. 13a). Both the Jaboncillo and Peral folds affect the Mesones Fm, but the T2 alluvial sheet is only visible in erosional channels passing through the folds. Thus, both folds were active after deposition of the Mesones Fm. The TUF4 ash, interbedded within the Las Tunas Fm, was deposited at ca. 0.6 Myr. Therefore, deposition of the Las Tunas Fm occurred after the T3 surface was abandoned. These results indicate a strong erosive period affecting the Mesones Fm before 0.6 Myr (Fig. 13b), followed by deposition of the Las Tunas Fm (Fig. 13c). This erosion was both vertical and lateral, creating a large space in the piedmont. Las Tunas Fm was deposited in this space, followed by incision to the T2 level. Then minor filling produced the T2 alluvial sheet. This has been followed by another vertical and lateral erosion of lesser amplitude, leading to the T1 bevelling and ending by the deposition of the T1 alluvial sheet. Then, final incision led to the modern T0. Both scenarios, investigated to explain the deep high ^{10}Be concentrations in T2 soil pit, suggest that part of the T2 alluvial layer has been mixed since ca. 60 kyr. This age is a maximum and corresponds to the smallest likely inheritance and the largest probable erosion rates based on geological arguments. This remobilization could be due to Las Tunas River avulsions during the alluvial T2-fan building.

Based on surface sample ^{10}Be and depth-profile analyses, both the T1 and T2 surfaces were abandoned by the river at the end of the last glaciation 20 $\pm$10 kyr ago, the error includes realistic uncertainties of both erosion rate (0–10 m Myr^{-1}) and inheritance (25000–120000 at g^{-1}). The ages obtained on the bedrock strath of T2, with unlikely inheritance and negligible erosion seem to date more precisely the abandonment of T2 at 15–20 kyr. Thus, only a short time span was necessary to incise the T2 surface (Fig. 13d), form the T1 strath level, deposit the T1 alluvial sheet, and incise it to the current river level around 100 m below the T2 surface (Fig. 13e). Finally, the mean millennial timescale erosion rate of the Santa Clara catchment was evaluated using sand from the active river channel at 0.30 $\pm$0.06 mm.yr^{-1}.

Climatic vs. tectonic effects on the entrenchment of the Las Tunas drainage

The Las Tunas region is located in an area of active tectonics, and deformation rates can be quantified using our data. The mean uplift rate on the Jaboncillo fold can be evaluated over two different time periods. First, the altitude difference between the T3 deposit (at least 800 kyr) at the fold apex and the T2 deposit (ca. 20 kyr) in the valleys of the fold is up to 75 m (García, 2004). Thus, the minimum mean uplift rate corresponding to development of the Jaboncillo fold during the last million years is around 0.1 mm.yr^{-1}. Secondly, we determined the mean uplift rate over the last 8 Myr using the TUF1 age of 8.3 Myr (Angostura Fm) and its vertical deformation evaluated at ca. 800 m (García, 2004). During this period, the mean relative uplift rate of the Jaboncillo fold was also ca. 0.1 mm.yr^{-1}. These values are comparable to those of Verges *et al.* (2007), who estimated an uplift rate of the Salinas fold in the piedmont, 130 km north of Las Tunas (31°40 'S). Therefore, the uplift rate was around 0.4 mm.yr^{-1} based on the deformation of the Angostura strata deformation. The decrease in cumulative uplift of the piedmont fold from north to south is in accordance with the north to south propagation of the Frontal Cordillera (and thus the piedmont) in this area.

Our analysis does not allow to unambiguously identify the origin of the T3 incision as due to tectonic change, climate change or both. The scarp observed along the T3

toe argues for faulting and associated tectonic uplift. On the other hand, the abandonment of T3 before 0.8 Myr could correspond to the mid-Pleistocene change in glacial-interglacial frequency and magnitude (Pisias and Moore, 1981; Raymo *et al.*, 2006). This transition could have increased the frequency of large floods and favoured erosion.

Moreover, our results showed that abandonment of T3 was followed by the widespread erosion of the Mesones Fm. The base level of the Las Tunas River was significantly dropped before the deposition of the Las Tunas Fm, leading to vertical and horizontal erosion. The Las Tunas deposit has then re-filled the piedmont and was at least 100 m thick from the mountain front to ca. 10 km downstream. The river does not seem to have incised into bedrock on the piedmont during the duration of terrace formation, meaning that there may not have been any net incision over the last million years. If tectonic uplift were responsible for the incision from the T2 surface to T0 (ca. 100 m in 20 kyr in the piedmont apex), this would correspond to an unrealistic uplift rate of around 5 $mm.yr^{-1}$.

Despite the active tectonic context, the T1 and T2 abandonment ages are in accordance with major warming periods (post-glaciation) in the area. As suggested in some other places, at the time the global climate was warming, glaciers were melting and rainfall increased water and sediment fluxes in mountain catchments, possibly promoting entrenchment (Dühnforth *et al.*, 2008; Gabet *et al.*, 2008). As suggested by Dühnforth *et al.* (2008), during glacial advance, available sediments in the mountain catchment are more likely to be transported because of favourable hydrological conditions. This lead to periods of deposition in the flatter piedmont. According to these authors, a climate change to an interglacial stage could then be responsible for the entrenchment of the piedmont. Indeed, ice retreat in the upper part of the mountain catchment reveals smooth relief with cirques and hanging valleys, which promote sediment trapping and reduced sediment transport rates in the upper part of the catchment. Finally, the decrease in sediment flux to the mountain front promotes incision in the piedmont apex because it increases river transport capacity along this reach, where there is an easily eroded alluvial riverbed. Therefore, climate variability might be the primary driver for the deposition of both alluvial sheets and the entrenchment of the T1 and T2 surfaces.

Furthermore, the entrenchment between T2 and T1 cannot be due to a system response to local uplift because the terraces converge downstream (see Fig. 5c). Moreover, the longitudinal profile of T2 shows that it is undeformed along the system and in particular, undisturbed at the mountain front. This indicates that no localized tectonic deformation has occurred after T2 development. Thus, the variation in incision downstream along T1 and the knick point observed in the current T0 level are not consequences of local tectonics effects, but rather are due to variations in erosion.

The downstream convergence of the Las Tunas terraces indicates that incision propagated downstream toward the converging point. Therefore, entrenchment of the Las Tunas River did not begin at the piedmont toe. This outcome prevents the entrenchment from being interpreted as resulting from base-level fall or piedmont uplift, for example. The distinctive patterns of landscape incision driven by climate or uplift have been discussed in a recent modelling study (Wobus *et al.*, 2010). According to this study, incision driven by climate change is 'most commonly accompanied by downstream migrating waves of incision and decreases in channel gradient'. On the other hand, 'under most circumstances incision driven by tectonics will be accompanied by upstream migrating incision and increases in channel gradient'. The results of Wobus *et al.* (2010) and our observations of the downstream propagation of the incision indicate climate driven incision. Our TCN data suggests that incision occurred during the last 20 kyr, which is also proposed as a time of incision along the Diamante River (Baker *et al.*, 2009). Nevertheless, experimental and numerical models have shown that autogenic waves of incision and erosion can affect a piedmont alluvial apron (e.g. Carretier and Lucazeau, 2005; Nicholas and Quine, 2007; Kim and Jerolmack , 2008; Reitz *et al.*, 2010; Pepin *et al.*, 2010; Powell *et al.*, 2012), leading to a similar evolution as that described here. Given the uncertainty on the marker ages, it cannot be totally excluded that the observed erosion-sedimentation history has an autogenic component.

Our study of the Las Tunas system assesses the role of sedimentation-erosion waves in the dynamics of a mountain range/piedmont system. For instance, a post-T2 erosion wave incising the entire catchment-fan system is suggested by the continuity of the T2 surface from the piedmont toe up to 10 km within the mountain catchment. The current river presents a concave profile with a knick point at the mountain front, implying greater incision in the piedmont than in the mountain range. Such a geometry suggests that the entrenchment could have been initiated at the mountain front and then propagated both downstream in the piedmont and upstream in the mountain catchment. Carretier and Lucazeau (2005) described the evolution of a coupled catchment-fan model in response to climate change. This model predicts that if precipitation in the mountain increases, the piedmont river incision is deep and very rapid, and propagates toward the mountain range by forming a knick point. The knick point does not result from mountain uplift, but from the difference in erodibility between the soft alluvial basin and the resistant mountain basement. This process results in the amplification of climate-driven incision in the whole system. Our observations in the Las Tunas system are consistent with such a scenario.

Record of external changes in an uplifted vs. stable piedmont

The Diamante terraces, located 200 km south of the Las Tunas area, record at least five major entrenchments, the timing of which Baker *et al.* (2009) linked to successive Pleistocene and Holocene climatic variations. In contrast, the Las Tunas system records few external changes with long periods of continuous sedimentation and dramatic incisions. The difference between these two neighbouring systems may be due to a different tectonic setting. Although the deformation of the San Raphael Block in the piedmont may be responsible for the uplift of the Diamante catchment, the Las Tunas system is mostly an internally drained system located behind the active deformation front. The greater magnitude of incision observed along the Diamante River, which may be the result of relative uplift of that area of the piedmont, prevents the entrenchment from re-filling to the same level during each major climate cycle. Thus, terrace levels are continuously recorded in the Diamante River landscape. However, because the Las Tunas foreland has not been submitted to continuous uplift, the piedmont base level has remained the same (as shown by terrace convergence) and entrenchments could have been erased with time. In this case, only the major or most recent events remain visible in the landscape. This comparison supports the counter-intuitive idea that climatic signals are better recorded in uplifting piedmonts than in tectonically stable ones.

CONCLUSION

This study combined geomorphological field observations, kinematic GPS data, satellite and aerial imagery, $^{40}Ar/^{39}Ar$ dating and ^{10}Be analysis. Results allow us to better understand the origin of entrenchment in the Las Tunas system and to provide a detailed description of terrace organization, leading to the following conclusions:

(1) Terraces converge downstream with a probable abandonment onset at the mountain-piedmont transition or in the mountain. This geometry and the absence of terrace deformation excludes that incision has been driven by a distal base-level fall far away from the study area or by faulting at the mountain-piedmont transition. A climatic origin of this incision seems more likely, although the Las Tunas piedmont is located in a region with evidence of active deformation.
(2) Our calculations show that the main terrace abandonment phases took place before 0.85 Myr for T3 and around 20 kyr for T1 and T2. Post-20 kyr incision was very rapid within a few 1000 yr.
(3) ^{10}Be concentrations in depth profiles over gently dipping alluvial surfaces show evidence of mixing of the surface layer over more than 1.5 m depth. Thus, the possibility of significant mixing must be taken into account when trying to date such surfaces with surface samples.
(4) Erosion-sedimentation waves have affected the entire system from the piedmont toe to up to 10 km upstream of the mountain to piedmont transition. These waves are associated with large oscillations in river elevation (ca. 100 m), probably amplified by the coupling between the catchment and fan domains.
(5) Contrary to the neighbouring Diamante River system, where greater magnitudes of incision (possibly driven by piedmont uplift) have allowed better preservation of the Pleistocene terrace record, the Las Tunas system may only preserve a partial record of climate changes due to repeated incision and aggradation at similar elevations. This comparison suggests that Pleistocene climate changes are better recorded in uplifting than in stable piedmont landscapes.

APPENDIX

Calculating the mean $[^{10}Be]$

To determine the surface layer remobilization age, we use a method similar to Perg *et al.* (2001), consisting of integrating Eqn (1) between the two depths of the mixed layer. We improve the previous approach by taking into account all the terms of eqn 1, including the radioactive decay terms, the effect of the erosion rate and the relative contributions of neutrons and muons.

The mean concentration ($\bar{C}(t)$) of a surface layer located between depths H_1 and H_2 is evaluated using Eqn (A1):

$$\bar{C}(t) = C_0 \cdot e^{-\lambda t} + \frac{1}{H_2 - H_1} \sum \chi_i \cdot \int_{H_1}^{H_2} \left[\frac{P_0}{\lambda + \frac{\epsilon\rho}{\Lambda_i}} \cdot \left(1 - e^{-\left(\lambda + \frac{\epsilon\rho}{\Lambda_i}\right)t} \right) \cdot e^{-\frac{\rho x}{\Lambda_i}} \right] dx \quad (A3)$$

this leads to Eqn (A2):

$$\bar{C}(t) = C_0 \cdot e^{-\lambda t} + \sum \chi_i \frac{P_0 \cdot \left(e^{-\frac{H_1\rho}{\Lambda_i}} - e^{-\frac{H_2\rho}{\Lambda_i}}\right)}{\left(\lambda + \frac{\epsilon\rho}{\Lambda_i}\right) \cdot \frac{(H_2 - H_1)\rho}{\Lambda_i}} \cdot \left(1 - e^{-(\lambda + \frac{\epsilon\rho}{\Lambda_i})t}\right) \quad (A4)$$

We use a graphic resolution to solve this equation for t.

Fig. A

Step heating spectra of TUF4 $^{40}Ar/^{39}Ar$ analysis: A and B are the spectrum for the two consecutive runs. C is the age-probability spectrum of both runs. Error ranges are expressed with 2σ of confidence.

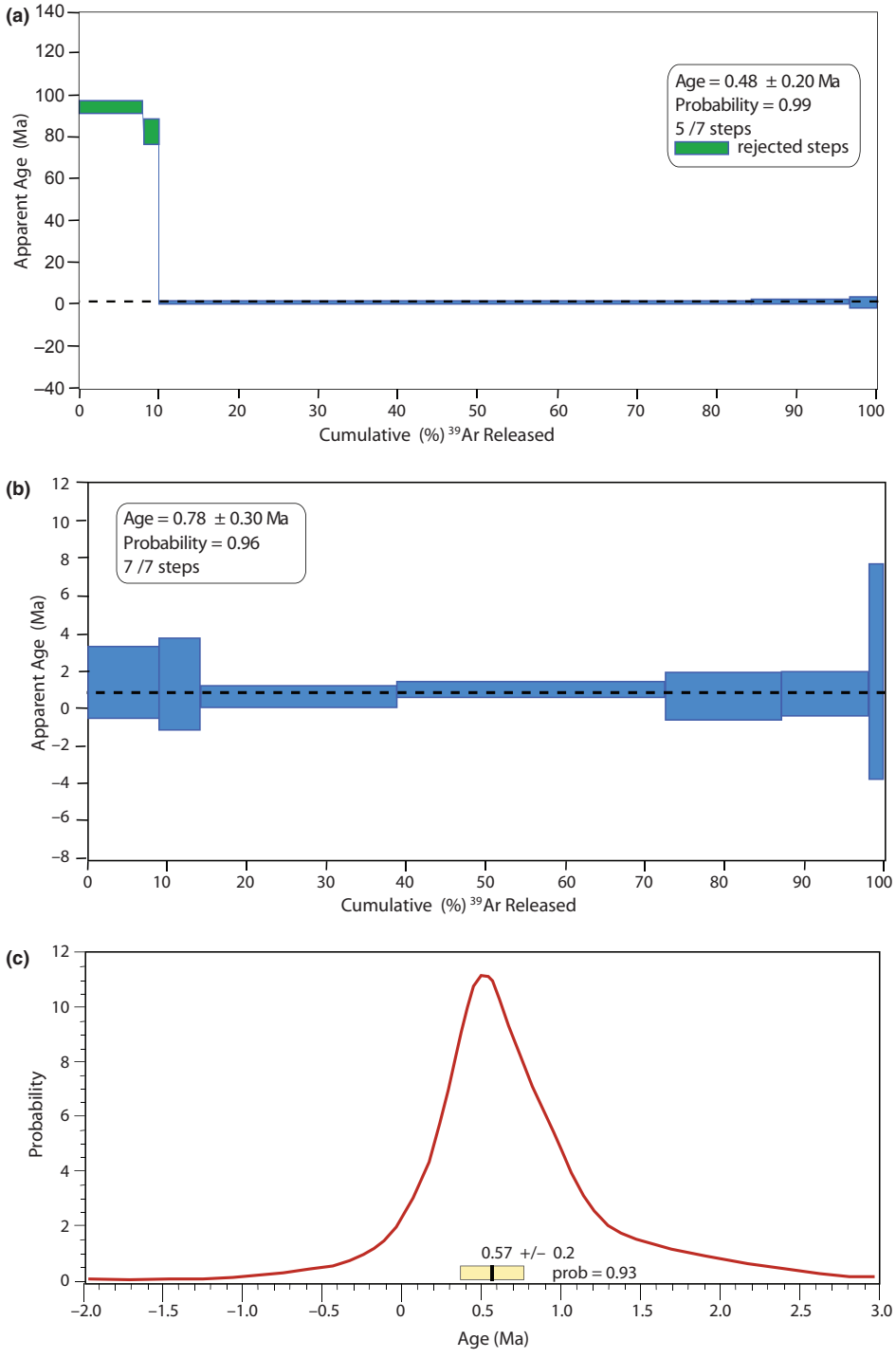

ACKNOWLEDGEMENTS

We thank H. Wittman and F. Von Blanckenburg for their kind help in the setup of the GET ^{10}Be Chemical preparation facility. We kindly thank J. Vargas for his help in sample sieving, C. Lagane for her help in quartz purification and the Regimiento de Infanteria de Montana 11 for their kind authorization of access to the military field area. Judit Ozoray and Sara Mullin corrected the language in the manuscript. Finally, A. Densmore, M. Dühnforth, S. Baker and the Editor P. van der Beek strongly improved this contribution.

REFERENCES

Anderson, R.S., Repka, J.L. & Dick, G.S. (1996). Explicit treatment of inheritance in dating depositional surfaces using in situ ^{10}Be and ^{26}Al. *Geology*, **24**, 47–51.

Armitage, J.J., Duller, A., Whittaker, A. & Allen, P.A. (2011) Transformation of tectonic and climatic signals from source to sedimentary archive. *Nat. Geosci.*, **4**, 231-235, DOI 10.1038/NGE0187.

Babault, J., Bonnet, S., Crave, A. & Van den Driessche, J. (2005) Influence of piedmont sedimentation on erosion dynamics of an uplifting landscape: an experimental approach. *Geology*, **33**(4), 301–304.

Baker, S., Gosse, J., McDonald, E., Evenson, E. & Martinez, O. (2009) Quaternary history of the piedmont reach of Rio Diamante, Argentina. *J. South Am. Ear. Sci.*, **28**, 54–73.

Balco, G., Stone, J.O., Lifton, N.A. & Dunai, T.J. (2008) A complete and easily accessible means of calculating surface exposure ages or erosion rates from ^{10}Be and ^{26}Al measurements. *Quat. Geochronol.*, **3-3**, 174–195.

Beaumont, P. (1972) Alluvial fans along the foothills of the Elburz Mountains, Iran. *Palaeogeography, Palaeoclimatol., Palaeoecol.*, **12**, 251–273.

Bierman, P., Clapp, E., Nichols, K., Gillespie, A. & Caffee, M. (2001) Using cosmogenic nuclide measurements in sediments to understand background rates of erosion and sediment transport. In: *Landscape Erosion and Evolution Modeling* (Ed. by R.S. Harmon& W.M. Doe), pp. 89–116. Kluwer 1., New York.

Blair, T. (1999a) Cause of dominance by sheetflood vs. debris-flow processes on two adjoining alluvial fans, death valley, California. *Sedimentology*, **46**, 1015–1028.

Blair, T. (1999b) Sedimentary processes and facies of the waterlaid anvil spring canyon alluvial fan, death valley, California. *Sedimentology*, **46**, 913–940.

Blair, T. (1999c) Sedimentology of the debris-fow-dominated warm spring canyon alluvial fan, death valley, California. *Sedimentology*, **46**, 941–965.

Blissenbach, E. (1954) Geology of alluvial fans in semi-arid regions. *Geol. Soc. Am. Bull.*, **65**, 175–190.

Braucher, R., Brown, E., Bourlès, D. & Colin, F. (2003) In situ produced ^{10}Be measurements at great depths: implications for production rates by fast muons. *Earth. Planet. Sci. Lett.* **211**, 251–258.

Braucher, R., Siame, L., Bourlès, D. & Colin, F. (2009) Determination of both exposure time and denudation rate from an in situ-produced ^{10}Be depth profile: a mathematical proof of uniqueness. Model sensitivity and applications to natural cases. *Quat. Geochronol.* **4**, 56–67.

Braucher, R., Merchel, S., Borgomano, J. & Bourlès, D.L. (2011) Production of cosmogenic radionuclides at great depth: a multi element approach. *Earth Planet. Sci. Lett.*, **309**, 1–9.

Brown, E.T., Stallard, R.F., Larsen, M., Raisebeck, G.M. & Yiou, F. (1995) Denudation rates determined from the accumulation of in situ-produced ^{10}Be in the Luquillo experimental forest, Puerto Rico. *Earth Planet. Sci. Lett.*, **129**, 193–202.

Bull, W. (1964) *Geomorphology of Segmented Alluvial Fans in Western Fresno County*. U.S. Geological Survey Professional Paper 352-E, California. pp. 89–129.

Cahill, T. & Isacks, B.L. (1992) Seismicity and shape of the subducted Nazca plate. *J. Geophys. Res.*, **97**, 17503–17529.

Carretier, S. & Lucazeau, F. (2005) How does alluvial sedimentation at range fronts modify the erosional dynamics of mountain catchments?. *Basin. Res.*, **17**, 361–381.

Charrier, R., Baeza, ., Elgueta, S., Flynn, J., Gans, P., Kay, S., Munoz, N., Wyss, A. & Zurita, E. (2002) Evidence for Cenozoic extensional basin development and tectonic inversion south of the flat-slab segment, southern Central Andes, Chile (33-36S.L). *J. of South Am. Ear. Sci.*, **15**, 117–139.

Chmeleff, J., von Blanckenburg, F., Kossert, K. & Jakob, D. (2010) Determination of the Be-10 half-life by multicollector ICP-MS and liquid scintillation counting. *Nucl. Instrum. Methods Phys. Res. B*, **263**(2), 192–199.

Clapperton, C. (1983) The glaciation of the Andes. *Quat. Sci. Rev.*, **2**, 83–155

Clarke, L., Quine, T.A. & Nicholas, A. (2010) An experimental investigation of autogenic behaviour during alluvial fan evolution. *Geomorphology*, **15**, 278–285.

Codilean, A. (2006) Calculation of the cosmogenic nuclide production topographic shielding scaling factor for large areas using DEMs. *Earth Surf. Proc. Land.*, **31**(6), 785–794.

Condom, T., Coudrain, A., Sicart, J. & Thiry, S. (2007) Computation of the space and time evolution of equilibrium-line altitudes on Andean glaciers (10°S). *Glob. Planet. Change*, **59**, 189–202.

Cristallini, E., Boggeti, D., Regazzoni, C., Anzulovich, L., Cerdan, J., Ayala, M., Scolari, J. & Leiro, F. (2000) *Cuenca Cuyana. Intrepretacion Estructural Regional*. Repsol-YPF, CONICET, Universidad de Buenos Aires, Buenos Aires, Argentina.

D'Antoni, H. (1983) Pollen analysis of Gruta del Indio. *Quat. South America Antarctic Peninsula*, **1**, 83–104.

Densmore, A., Allen, P. & Simpson, G. (2007) Development and response of a coupled catchment fan system under changing tectonic and climatic forcing. *J. Geophys. Res.*, **112**, F01002, doi:10.1029/2006JF000474.

Dühnforth, M., Densmore, A., Ivy-Ochs, S. & Allen, P. (2008) Controls on sediment evacuation from glacially modified and unmodified catchments in the eastern Sierra Nevada, California. *Earth Surf. Proc. Land.*, **33**, 1602–1613.

Eckis, R. (1928) Alluvial fans of the Cucamonga district southern California. *J. Geol.*, **36**, 224–247.

Espizua, L. (1999) Chronology of late Pleistocene glacier advances in the rio Mendoza valley, Argentina. *Glob. Planet. Change*, **22**, 193–200.

Espizua, L. (2004) Pleistocene glaciations in the Mendoza Andes, Argentina. In: *Quaternary Glaciations – Extent and Chronology* (Ed. by Ehlers, J. & Gibbard, P.), pp. 69–73. Elseviers III, Cambridge.

Farías, M., Charrier, Carretier, S., Martinod, J., Fock, A., Campbell, D., Caceres, J. & Comte, D. (2008) Late Miocene high and rapid surface uplift and its erosional response in the Andes of Central Chile (33–35S). *Tectonics*, **27**, TC1005. doi:10.1029/2006TC002046

Farías, M., Comte, D., Charrier, R., Martinod, J., David, C., Tassara, A., Tapia, F. & Fock, A. (2010) Crustal-scale structural architecture in central Chile based on seismicity and surface geology: implications for Andean mountain building. *Tectonics*, **29**, TC3006. doi:10.1029/2009TC002480

Farr, T., Rosen, P., Caro, E., Crippen, R., Duren, R., Hensley, S., Kobrick, M., Paller, M., Rodriguez, E., Roth, L., Seal, D., Shaffer, S., Shimada, J., Umland, J., Werner, M., Oskin, M., Burbank, D. & Alsdorf, D. (2007) The

Shuttle Radar Topography Mission Rev. *Geophysics*, **45**, RG2004, doi: 10.1029/2005RG000183.

Gabet, E., Burbank, D., Pratt-Sitaula, B. & Putkonen, J. (2008) Modem erosion rates in the High Himalayas of Nepal. *Earth Planet. Sci. Lett.*, **267**(3-4), 482–494.

García, V. (2004) Analisis Estructural y Neotectnico de las Lomas Jaboncillo y del Perral, Departamento de Tupungato, Provincia de Mendoza. Licenciatura, Facutad de ciencias Exactas y Naturales, Universidad de Buenos Aires.

Giambiagi, L., Ramos, V., Godoy, E., Alvarez, P.P. & Orts, S. (2003) Cenozoic deformation and tectonic style of the Andes, between 33 and 34 South latitude. *Tectonics*, **22-4**, 1041, doi:10.1029/2001TC001354.

Giambiagi, L., Tunik, M.A. & Ghiglione, M. (2001) Cenozoic tectonic evolution of the alto tunuyán foreland basin above the transition zone between the flat and normal subduction segment (33° 30'–34°), western Argentina. *J. South Am. Ear. Sci.*, **14**, 701–724.

Granger, D., Kircher, J. & Finkel, R. (1996) Spatially averaged long-term erosion rates measured from in situ-produced cosmogenic nuclides in alluvial sediment. *J. Geol.*, **104**, 249–257.

Harrison, S. (2004) The Pleistocene glaciations of Chile. In: *Quaternary Glaciations – Extent and Chronology* (Ed. by J., Ehlers & P., Gibbard), pp. 89–103. Vol. **III**. Elseviers, Amsterdam.

Harvey, A. (1999) The impact of quaternary sea-level and climatic change on coastal alluvial fans in the Cabo de Gata ranges, southeast Spain. *Geomorphology*, **28**, 1–22.

Heimsath, A.M., Chappell, J., Spooner, N.A. & Questiaux, D.G. (2002) Creeping soil. *Geology*, **30–2**, 111–114.

Hoffmann, J. (1975) Atlas climàtico de América del Sur: scales 1:10,000,000 and 1:50,00,000. World Meteorological Organization 28.

Hooke, R (1968) Steady-state relationships on arid region alluvial fans in closed basins. *Am. J. Sci.*, **266**, 609–629.

Humphrey, N., Heller, P. (1995) Natural oscillations in coupled geomorphic systems: an alternative origin for cyclic sedimentation. *Geology*, **23**, 499–502.

Irigoyen, M.V., Buchan, K.L., Villeneuve, M.E. & Brown, R.L. (2002) Cronologı`a y significado tectònico de los estratos sinorogènicos neògenos aflorantes en la regiòn de Cacheuta-Tupungato, provincia de Mendoza. *Asociaciòn Geològica Argentina*, **57**(1), 3–18.

Kim, W. & Jerolmack, D. (2008) The pulse of calm fan deltas. *J. Geol.*, **116**(4), 315–330.

Korschinek, G., Bergmaier, A., Dillmann, I., Faestermann, T., Gerstmann, U., Knie, K., von Gostomski, C., Maiti, M., Poutivtsev, M., Remmert, A., Rugel, G. & Wallner, A. (2009) Determination of the Be-10 half-life by HI-ERD and liquid scintillation counting. *Geochim. Cosmochim. Acta*, **73**, A685.

Kull, C., Imhof, S., Grosjean, M., Zech, R. & Veit, H. (2008) Late Pleistocene glaciation in the Central Andes: temperature versus humidity control: a case study from the eastern Bolivian Andes (17° S) and regional synthesis. *Glob. Planet. Change*, **60**, 148–164.

Lavé, J. & Avouac, J.-P. (2001) Fluvial incision and tectonic uplift across the Himalayas of central Nepal. *J. Geophys. Res.*, **106-B11**, 26, 561–26, 591.

Le Dortz, K., Meyer, B., Sebrier, M., Braucher, R., Nazari, H., Benedetti, L., Fattahi, M., Bourlès, D., Foroutan, M., Siame, L., Rashidi, A. & Bateman, M.D. (2011) Dating inset terraces and offset fans along the Dehshir Fault (Iran) combining cosmogenic and OSL methods. *Geophys. J. Int.*, **185**, 1147–1174.

Mehl, A.E. & Zárate, M.A. (2012) Late Pleistocene and Holocene environmental and climatic conditions in the eastern Andean piedmont of Mendoza (33–34S, Argentina). *J. South Am. Ear. Sci.*, **37**, 41–59.

Merritts, D.J., Vincent, K.R. & Wohl, E.E. (1994) Long river profiles, tectonism, and eustasy: a guide to interpreting fluvial terraces. *J. Geophys. Res.*, **99**, 14,031–14,050.

Muto, T. & Steel, R.J. (2004) Autogenic response of fluvial deltas to steady sea-level fall: implications from flume-tank experiments. *Geology*, **32**, 401–404.

Nicholas, A. & Quine, T. (2007) Modeling alluvial landform change in the absence of external environmental forcing. *Geology*, **35**, 527–530.

Ono, Y. (1990) Alluvial fans in Japan and South Korea. In: *Alluvial Fans: A Field Approach* (Ed. by A.H. Rachocki & M. Church) pp. 247–269. J. Wiley and Sons Ltd, New York.

Pepin, E., Carretier, S. & Hérail, G. (2010) Erosion dynamics modelling in a coupled catchment-fan system with constant external forcing. *Geomorphology*, **122**, 78–90.

Perg, L., Anderson, R. & Finckel, R. (2001) Use of a new $^{1}0Be$ and $^{2}6Al$ inventory method to date marine terraces, Santa Cruz, California, USA. *Geology*, **29-10**, 879–882.

Pisias, N. & Moore, T. (1981) The evolution of the Pleistocene climate: a time series approach. *Earth Planet. Sci. Lett.*, **52**, 450–458.

Poisson, B. & Avouac, J.-P. (2004) Holocene hydrological changes inferred from alluvial stream entrenchment in North Tian Shan (Northwestern China). *J. Geol.*, **112**, 231–249.

Polanski, J. (1963) Estatigrafia, Neotectonica y Geomorphologia del Pleistoceno pedemontano entre los rios Diamante y Mendoza, provincia de Mendoza. *Rev. Asoc. Geol. Argent.*, **17-3/4**, 127–349.

Powell, E., Kim, W. & Muto, T. (2012) Varying discharge controls on timescales of autogenic storage and release processes in fluvio-deltaic environments: tank experiments. *J. Geophys. Res.*, **117**, F02011, doi:10.1029/2011JF002097..

Quigley, M., Sandiford, M. & Cupper, M. (2007) Distinguishing tectonic from climatic controls on range-front sedimentation. *Basin Res.*, **19**, 491–505.

Ramos, V.A., Cristallini, E.O. & Pérez, D.J. (2002) The Pampean flat-slab of the central Andes. *J. South Am. Ear. Sci.*, **15** (1), 59–78.

Raymo, M., Lisiecki, L. & Nisancioglu, K. (2006) Plio-Pleistocene ice volume, antarctic climate, and the global $d^{1}8o$ record. *Science*, **313**, 492–495.

Regard, V., Bellier, O., Braucher, R., Gasse, F., Bourlès, D., Mercier, J., Thomas, J., Abbassi, M., Shabanian, E. & Soleymani, S. (2006) $^{1}0$Be dating of alluvial deposits from southeastern Iran (the Hormoz Strait area). *Palaeogeography Palaeoclimatol. Palaeoecol.*, **242**, 36–53.

Reitz, M.D., Jerolmack, D.J. & Swenson, J.B. (2010) Flooding and flow path selection on alluvial fans and deltas. *Geophys. Res. Lett.*, **37**, L06401.

Ritz, J.-F., Vassallo, R., Braucher, R., Brown, E.T., Carretier, S. & Bourlès, D.L. (2006) Using in situ produced ^{10}Be to quantify active tectonics in the Gurvan Bogd mountain range (Gobi-Altay, Mongolia). *GEOL S AM S.*, **415**, 87–110.

Siame, L. & Bellier, O. (2006) A seismotectonic model for the Argentine Precordillera and the western Sierras Pampeanas. *Rev. Asoc. Geol. Argent.*, **61**(4), 604–619.

Siame, L., Bellier, O., Braucher, R., Sébrier, M., Cushing, M., Bourlès, D., Hamelin, B., Baroux, E., de Voogd, B., Raisbeck, G. & Yiou, F. (2004) Local erosion rates versus active tectonics: cosmic ray exposure modelling in Provence (south-east France). *Earth. Planet. Sci. Lett.*, **220**, 345–364

Siame, L., Bellier, O., Sébrier, M. & Araujo, M. (2005) Deformation partitioning in flat subduction setting: the case of the Andean foreland of Western Argentina (28S). *Tectonics*, **24**, TC5003, doi:10.1029/2005TC001787.

Siame, L., Braucher, R. & Bourlès, D. (2000) Les nucléides cosmogéniques produits in-situ: de nouveaux outils en géomorphologie quantitative. *Bull. Soc. Géol. France*, **171**, 383–396.

Singh, V. & Tandon, S. (2010) Integrated analysis of structures and landforms of an intermontane longitudinal valley (Pinjaur Dun) and its associated mountain fronts in the NW Himalaya. *Geomorphology*, **114**, 573–589.

Smith, J.A., Seltzer, G.O., Rodbell, D.T. & Klein, A.G. (2005) Regional synthesis of last glacial maximum snowlines in the tropical Andes, South America. *Quat. Int.*, **138-139**, 145–167.

Staley, D.M., Wasklewicz, T.A. & Blaszczynski, J.S. (2006) Surficial patterns of debris flow deposition on alluvial fans in Death Valley, CA using airborne laser swath mapping data. *Geomorphology*, **74**, 152–163.

Stauder, W. (1975) Subduction of the Nazca plate under Peru as evidenced by focal mechanism and by seismicity. *J. Geophys. Res.*, **80**, 1053–1064.

Stone, J. (2000) Air pressure and cosmogenic isotope production. *J. Geophys. Res.*, **105**, 23753–23759.

Tucker, G.E. & Slingerland, R. (1997) Drainage basin responses to climate change. *Wat. Resour. Res.*, **33**, 2031–2047.

Verges, J., Ramos, V.A., Meigs, A., Cristallini, E., Bettini, F.H. & Cortés, J.M. (2007) Crustal wedging triggering recent deformation in the Andean thrust front between 31° S and 33° S: Sierras Pampeanas-Precordillera interaction. *J. Geophys. Res.*, **112**, B03S15, doi:10.1029/2006JB004287.

Viseras, C., Calvache, M., Soria, J. & Fernandez, J. (2003) Differential features of alluvial fans controlled by tectonic or eustatic accommodation space. Examples from the Betic Cordillera, Spain. *Geomorphology*, **50**, 181–202.

Volker, H., Wasklewicz, T. & Ellis, M. (2007) A topographic fingerprint to distinguish alluvial fan formative processes. *Geomorphology*, **88**, 34–45.

Von Blanckenburg, F., Belshaw, N., O' Nions, R. (1996) Separation of ^{9}Be and cosmogenic $^{1}0Be$ from environmental and SIMS isotope dilution analysis. *Chemical Geology*, **129**(1,2), 93–99.

Whipple, K.X., Dunne, T. (1992) The influence of debris-flow rheology on fan morphology, Owens valley, California. *Geol. Soc. Am. Bull.*, **104**, 887–900.

White, K. (1991) Geomorphological analysis of piedmont landforms in the Tunisian Southern Atlas using ground data and satellite imagery. *Geogr. J.*, **157**, 279–294.

Wobus, C.W., Tucker, G., Anderson, R. (2010) Does climate change create distinctive patterns of landscape incision? *J. Geophys. Res.*, **115**, F04008, doi:10.1029/2009JF001562.

Zárate, M. (2002) Geología y estratigrafía del Pleistoceno Tardio-Holoceno en el piedemonte de Tunuyán-Tupungato, Mendoza, Argentina. In: *XV Congreso Geolgico Argentino, El Calafate* (Ed. by N., Cabaleri, C., Cingolani, E., Linares, M., Lpez de Luchi, H., Ostera, and H., Panarello) pp. 615–620. ACTAS II, Santa Cruz, Argentina.

Zárate, M. & Mehl, A. (2008) Estratigrafá y geocronologá de los dépositos del Pleistoceno tardó-Holoceno de la cuenca del Arroyo la Estacada, departamentos de Tunuyán y Tupungato (valle del Uco), Mendoza. *Rev. Asoc. Geol. Argent.*, **63**(3), 407–416.

Zech, R., May, J., Kull, C., Ilgner, J., Kubik, P. & Veit, H. (2008) Timing of the late quaternary glaciation in the Andes from around 15 to 40°S. *J. Quatern. Sci.*, **23**(6-7), 635–647.

Manuscript received 16 January 2012; In revised form 01 July 2012; Manuscript accepted 07 December 2012.

